2011

A Gis Investigation of Regional Geologic Controls on Mercury Deposits in the Southwest Region of Arkansas

Lindsey Carol Langsdon

A GIS INVESTIGATION OF REGIONAL GEOLOGIC CONTROLS ON MERCURY DEPOSITS IN THE SOUTHWEST REGION OF ARKANSAS

A Thesis
Presented in partial fulfillment of requirements
for the degree of Master of Science
in the Department of Geology and Geological Engineering
The University of Mississippi

by

Lindsey C. Langsdon

August 2011

ABSTRACT

The mercury district of southwest Arkansas, located within Clark, Pike, and Howard counties, contains 77 mapped mercury deposits, primarily in the form of cinnabar, found within the sandstones and shales of the Stanley and Jackfork Formations. The geographic locations of the majority of the deposits tend to form an east-northeast alignment in map view. Utilization of Geographic Information Systems (GIS) tools provided insight to the regional controls on the spatial distribution of the mercury deposits by examining the proposed relationships between mercury deposits and regional faults or changes in lithology, both of which have been suggested (Clardy and Bush, 1976) to explain the narrow band of permissive host rock for the deposits. GIS was used to determine which mode of deposition (structural features or lithologic changes) better explains the linear depositional pattern of mercuric minerals within the region by examining which potential control mechanism is closer to the deposit locations. The goal was accomplished by mapping the regional thrust faults and changes in lithology at an appropriate scale. Lithologic units were mapped using decision tree learning methods and a methodology, developed by Belt and Paxton (2005), dependant on topographic attributes unique to each rock type. A composite map of the changes in lithology, regional thrust faulting, and the deposits themselves were used to determine which of the suggested relationships exerts more control on the placement of the deposits by being physically closer. Investigation revealed that the faulting is the most controlling feature, on average, and that a regional variation in controlling mechanism exists. Within regions dominated by sandstone, contacts are the more controlling feature. Within shale dominated regions, the faults are the prevailing control feature.

DEDICATION

To my wonderful parents,

Who have guided, encouraged, and loved me for my entire life.

Without them, this would have never been possible.

Love,

Lindsey

LIST OF ABBREVIATIONS

Geographic Information Systems (GIS)

Digital Elevation Model (DEM)

Waikato Environment for Knowledge Analysis (WEKA)

True Positive (TP)

False Positive (FP)

ACKNOWLEDGEMENTS

I would like to acknowledge the University of Mississippi Geoinformatics Center (UMGC), a Mississippi Mineral Resources Institute (MMRI) program for providing funding and education, as well as resources to complete this project. For the past three years the UMGC program and staff have supported me. I would also like to thank Dr. Greg Easson, director of MMRI, as well as Hal Robinson, associate director of UMGC, for educating me throughout the entirety of this project. I would also like to acknowledge the Department of Geology and Geological Engineering at the University of Mississippi for providing me with funding, as well as many hours of mentoring. I would also like to thank Steven Fox, for encouraging me every step of the way. Lastly, and most importantly, I would like to thank my committee members, Dr. Terry Panhorst, Dr. Greg Easson, and Dr. Henrique Momm, for the many hours of mentoring and advising that they have provided me with. Without them, this project would not have been possible.

TABLE OF CONTENTS

LIST OF TABLES

LIST OF FIGURES

LIST OF APPENDICES

CHAPTER 1. INTRODUCTION

1.1 Location and History

The mercury district of southwest Arkansas is within Clark, Pike, and Howard counties, all in the southwest region of Arkansas (Figure 1). This district is found within the Athens Plateau physiographic province of the Ouachita Mountains (Clardy and Bush, 1976).

Figure 1.
The mercury district (outlined in red) in southwest Arkansas.

The Athens Plateau is between the southern boundary of the central portion of the Ouachita Mountains (Figure 2), which is part of the Novaculite Uplift, and the Gulf Coastal Plain (Branner, 1932).

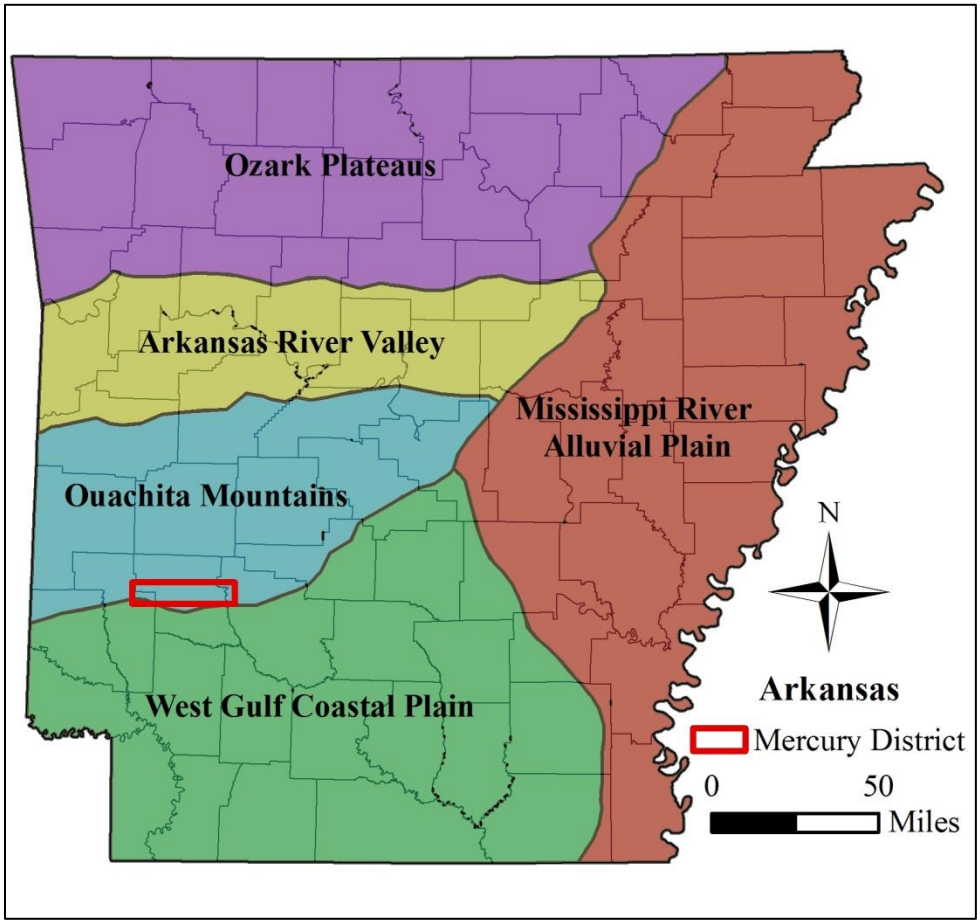

Figure 2.
Physiographic provinces of Arkansas (Arkansas Geological Commission, 2010). Location of the Arkansas mercury district indicated by the red rectangle.

The district, as it is presently defined, is approximately 30 miles long and 6 miles wide. Cinnabar deposits found near the western edge of the district are located in section 13, T7S, R27W, eastward to section 6, T7S, R22W (Clardy and Bush, 1976).

Cinnabar was first discovered, but not identified, in the district in 1930 at a Missouri Pacific Railroad quarry, located in section 28, T6S, R23W (Reed and Wells, 1938). Several

more discoveries were made throughout the next year and a half. It was not until the Arkansas state geologist, George C. Branner, publicized the discoveries on August 30, 1931 that the mining development of the district began (Reed and Wells, 1938). From 1931 until 1946 the district was heavily mined and developed, producing nearly 11,400 flasks (each at 76 pounds) of mercury (Stone and Bush, 1984). Over 100 surface exposures were documented by various small companies and investigators of the region (Clardy and Bush, 1976). There are 77 mapped mercury occurrences in the district.

1.2 Study Purpose

Mercury deposits within the district have a distinct surface expression in map view. The geographic locations of the majority of the 77 mapped mercury deposits tend to form an east-northeast alignment (Figure 3), similar to the regional geologic and topographic grain.

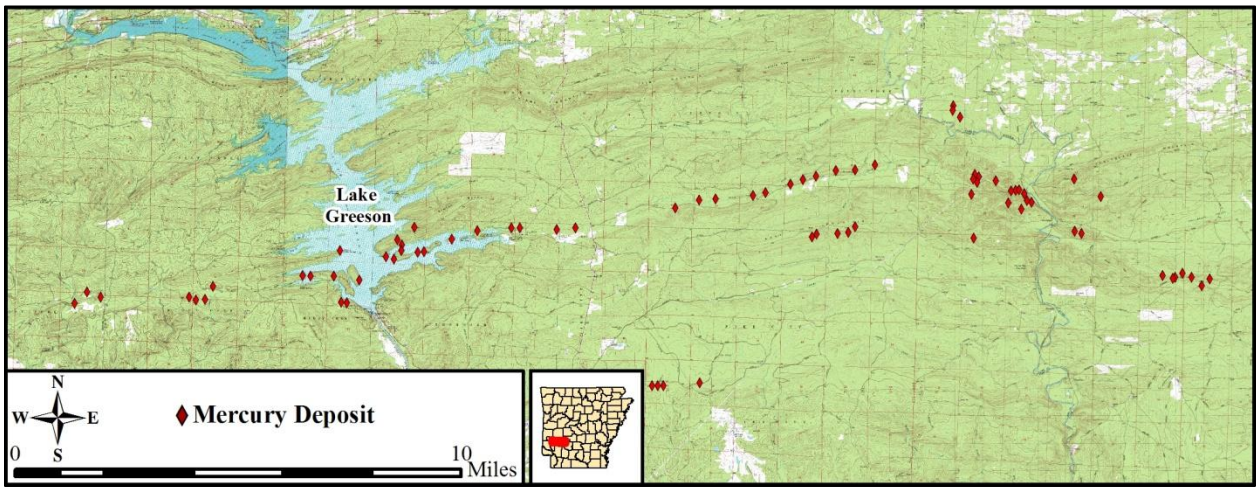

Figure 3.
Map of the mercury deposits (shown as red diamonds) within the Arkansas mercury district. Note the majority of these deposits occur in an east-northeast alignment.

Since the most recent investigations of these deposits in the mid-1970s, many scientific advances have occurred in Geographic Information Systems (GIS). Utilization of these tools can provide insight to the regional controls on the spatial distribution of the cinnabar deposits by examining

the proposed relationships between mercury deposits and regional thrust faults or changes in lithology, both of which have been suggested (Clardy and Bush, 1976) to explain the narrow band of permissive host rock for the deposits.

CHAPTER 2. GEOLOGY

2.1 Regional Geology

The rock types which host the mercury mineralization are Paleozoic. The Pennsylvanian Jackfork Formation hosts the majority of the deposits, while the Mississippian Stanley Formation hosts the remainder of the deposits (Clardy and Bush, 1976). These formations have been deformed by southward-dipping thrust fault zones resulting from what has been interpreted as part of a subduction complex (Viele, 1979). The region is comprised of a series of anticlines and synclines which trend east-west (Clardy and Bush, 1976). The deformation in the area occurred during the Alleghanian orogeny, creating the Appalachian-Ouachita fold-thrust belt (Hatcher et al., 1989). As a result of the deformation in the area, the Paleozoic host beds dip steeply to the south (Clardy and Bush, 1976).

Also present in the district, but not host to the mercury mineralization, is the Pennsylvanian Atoka Formation and the Pennsylvanian Johns Valley Formation (from younger to older), which lie above the Jackfork Formation (Clardy and Bush, 1976). Other surface rocks within the region include relatively undeformed, gently dipping Cretaceous sediments of the Gulf Coastal Plain which overlap the folded and steeply dipping sandstones and shales along the southern border of the mercury district. These Cretaceous sediments include gravel, sand, clay, and limestone. Quaternary alluvium is within the areas where major streams are present, and is comprised typically of unconsolidated sand, gravel, and clay (Clardy and Bush, 1976).

Shales of the Stanley Formation make up the majority of surface rock in the Athens Plateau area. The Stanley Formation is nearly 6,000 feet thick in the district (Miser and Purdue, 1929). This formation is composed of about 75% shale and 25% sandstone. The shale is black, fissile, and readily weathers to a green and reddish color (Miser and Purdue, 1929). Bedding within the Stanley Formation is often very hard to determine due to the intense foliation developed during deformation. Sandstone in the Stanley Formation varies from a greenish gray to gray color with fine to medium-grained quartz sand. The Stanley Formation also tends to have minor amounts of white angular feldspar grains; some quartz and chert pebbles are also present in places (Clardy and Bush, 1976). The Stanley Formation contains three major sandstone units, of which all three are ore-bearing (Figure 4).

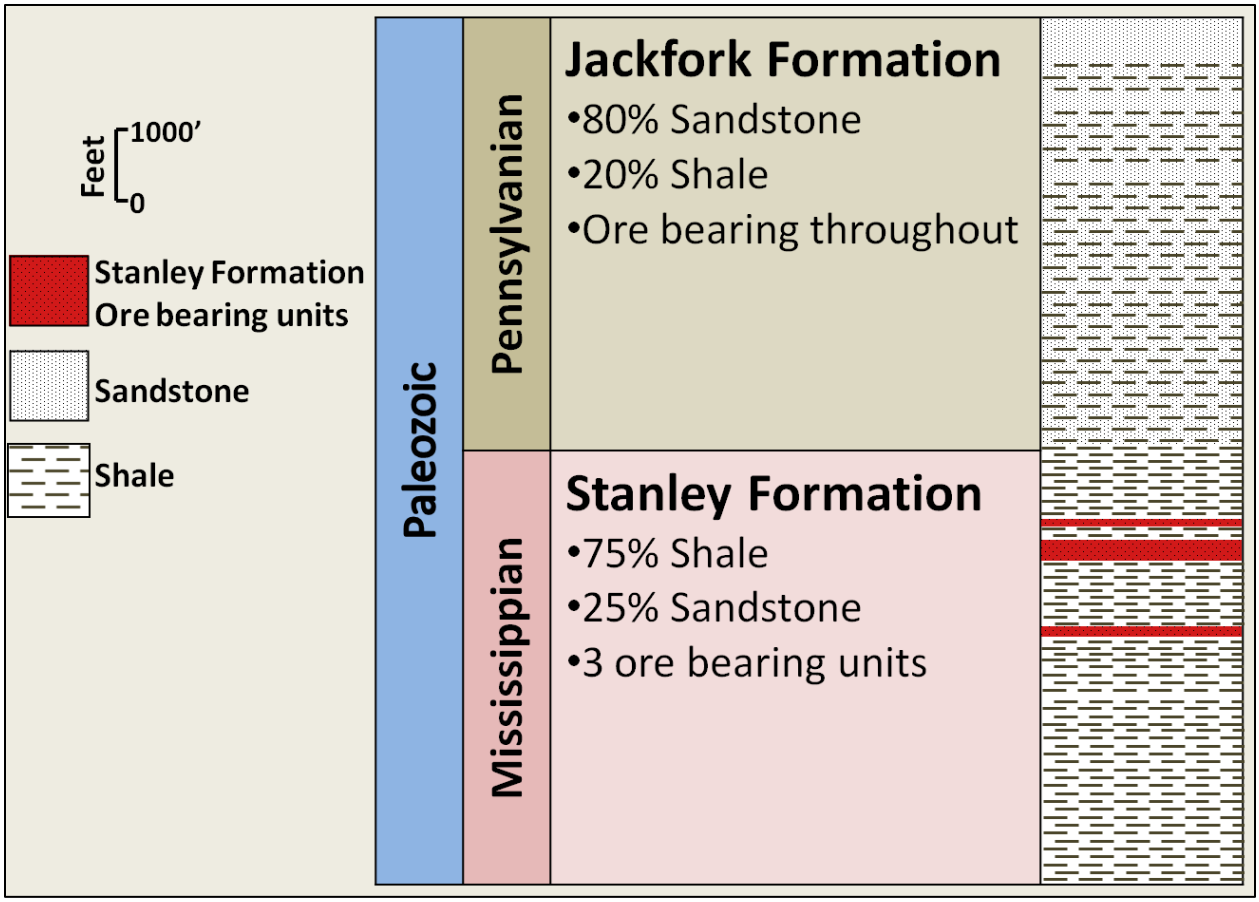

Figure 4.
Generalized stratigraphic column of the Jackfork and Stanley Formations. The Jackfork Formation is ore bearing throughout, while the Stanley Formation contains three major ore bearing units (highlighted in red).

The first sandstone unit, nearly 1,000 feet from the stratigraphic top of the Stanley Formation, is about 100 feet thick. Separated by 150 feet of shale below the base of the first unit is the second sandstone unit, composed of 300 feet of sandstone. The third unit, located more than 1,000 feet below the second unit, is comprised of 160 feet of sandstone (Gallagher, 1942). The first and second units of sandstone, along with the intervening 150 feet of shale, are together known as the Gap Ridge Sandstone Member. The third and lowest unit of 160 feet of sandstone is known as the Parker Hill Sandstone Member (Stearn, 1935).

The Jackfork Formation is conformable to the stratigraphically underlying Stanley Formation and is nearly 6,000 feet thick (Miser and Purdue, 1929). The Jackfork Formation is comprised of 80% sandstone and 20% shale (Reed and Wells, 1938). Sandstone layers range from inches to 20 feet thick in some sections with interbedded layers of shale ranging from an inch to 100 feet thick (Figure 4). Shale in the Jackfork Formation is typically gray to gray-black, and when present may appear in alternating layers of light brown to yellow and gray to gray-black shale (Reed and Wells, 1938). Reed and Wells (1938) describe the shale in this formation as "ribbonlike," because of the alternating colors banded in one section. The sandstone of the Jackfork Formation is typically a medium to coarse-grained quartz sand with a light gray color on fresh exposures (Clardy and Bush, 1976). The sandstone units contain some conglomerate near their top. The weathered portions of the sandstone are soft and light gray to yellow-brown (Clardy and Bush, 1976).

2.2 Topography and Geomorphology

The rock types in the district play a large role in the topography and geomorphology in this region. Shales of the Stanley Formation comprise most of the broad lowlands and valleys between the higher ridges, which are formed by the more competent sandstone members of the Jackfork Formation (Clardy and Bush, 1976). The alternating ridges and lowlands have a trend of approximately N 80° E and a varying relief of 100 to 350 feet. The dominant drainage pattern in the area is a trellis pattern of small streams, with two major southward-flowing rivers: the Little Missouri River and Antoine Creek. These two rivers are fed by east-west tributaries which flow between sandstone ridges within the Jackfork Formation. In certain places the sandstone is cut by the two major streams in the area, which is attributed to the regional faulting and deformation (Branner, 1932).

2.3 Regional Tectonic History

The Ouachita orogenic belt exposures of this area in southwest Arkansas represent only a small part of a larger tectonic event within Appalachian-Ouachita orogen (Viele, 1989). The mercury district in Arkansas is hosted in one set of exposures of the Ouachita orogenic belt, which begins around the southwest border of Texas, where it is exposed, and continues into the subsurface until it is exposed again in regions of Oklahoma and Arkansas, where it once again extends down into the subsurface and terminates in regions of Mississippi (Viele, 1989). The belt is nearly 2,100 km long, and approximately 80% of its entirety is buried by undeformed Mesozoic and Tertiary sediments deposited in the Mississippi Embayment of the Gulf Coastal Plain (Viele, 1989; Thomas, 1989). The Ouachita orogenic belt is composed of deformed Paleozoic rocks that once bordered the southern extent of the North America craton. The base of the Ouachita orogenic belt is part of a decollement, placing allochthonous Ouachita rocks over North America basement strata. The upper surface of the allochthonous Ouachita rocks is marked by an erosional surface of low relief. After the deposition and erosion of the upper surface of allochthonous rock, the deposition of the Gulf Coastal Plain ensued (Viele, 1989).

The "Ouachita facies" are the two major stratigraphic units which make up the orogenic belt, one lower and one upper unit (Viele, 1989). The environment in which these strata were deposited once bordered the Arkoma and Black Warrior foreland basins adjacent to the Appalachian-Ouachita thrust belts (Thomas, 1989). The lower of the two units is composed of shale, sandstone, micrite grading upward into "ribbonlike" chert, siliceous shale, and massive novaculite beds. This lower unit is Late Cambrian to Early Mississippian and ranges from 3-3.5 km thick. The lower unit of the Ouachita facies is termed the "off-shelf facies of pre-orogenic rocks" (Viele, 1989). The upper Ouachita facies units were deposited during the Ouachita

orogeny, and are termed "synorogenic" strata. These strata are composed of shelf-delta clastic wedge deposits and deep-water clastic wedge deposits (Viele, 1989). The age of the upper unit is Mississippian to Pennsylvanian (Thomas, 1989). The Stanley and Jackfork Formations are part of the synorogenic strata found in the upper unit of the Ouachita stratigraphic sequence (Morris, 1989).

2.4 Nature of the Mercury Deposits

The mercury found in the deposits in this district is restricted to the Mississippian Stanley Formation and the Pennsylvanian Jackfork Formation (Clardy and Bush, 1976). Cinnabar (HgS) is the only primary mercury ore found within the district; however, native mercury, metacinnabar, eglestonite, livingstonite, and calomel, are also found as secondary ore. Other sulfide minerals occurring within the region include: pyrite, stibnite, stibiconite, and galena. Primary gangue minerals found within the district include: dickite, quartz, siderite, barite, and calcite. Secondary gangue minerals found within the region include: iron oxides and hydroxides (limonite, goethite, and hematite), and opal (Clardy and Bush, 1976). Stearn (1936) lists the varying forms of mercury mineralization within the district: fracture filling, breccia filling, fault gouge, shale contact impregnation, vein mineralization, and as local disseminations in sandstones. Open space fillings and fracture coatings are also common (Clardy and Bush, 1976).

Mercury deposits in the district typically occurs as pipelike bodies associated with minor folds and cross faults in the region, although mineralization is also found as tabular bodies which are related to an individual sandstone bed or group of beds (Clardy and Bush, 1976). Sandstone beds located adjacent to shale beds are also permissive to the deposition of cinnabar. The sandstone was found to be more deformed in these areas, leaving openings for which mineralization to take place. It is also theorized by Stearn (1936) that shale beds, being

impervious to mineralizing solutions, provided an avenue for the mineralizing fluids to travel along. The mineralizing solutions are believed to have moved upwards via a thrust fault and deposited within the sandstone units of both the Stanley Formation and the Jackfork Formation (Stearn, 1936). It is suggested by Reed and Wells (1938) that the ore-bearing solutions came up in the fractured zones developed above the two major east-west thrust faults in the area and deposited in the fractures of the hosting units. All of the known mercury mineralization in the area is found in folded and faulted east-west anticlines and synclines. Clardy and Bush (1976) believe that the mineralizing fluids originated from igneous bodies to the south, and these fluids traveled northward to be deposited in the overthrusted fault blocks in the area. These same authors propose Cretaceous origins for the deposition of mercury in this area because the majority of igneous activity that led to quartz vein deposition in the region occurred at that time.

The geographic location of mercury deposits found within the region display a relatively tight linear alignment (Figure 3). The surface expression of these deposits may represent a broader regional control mechanism. Proposed explanations of the mercury deposit surface locations have been offered by several authors, with the common theory that the deposits occur in this fashion because mineralizing fluids traveled up major thrust faults within the region and dispersed through shattered zones (Clardy and Bush, 1976; Stearn, 1936; Hansell and Reed, 1935).

CHAPTER 3. METHODOLOGY

The alignment of mercury deposits within southwest Arkansas have been suggested to be the result of regional thrust faulting and/or regional lithologic changes between sandstone and shale within the Stanley and Jackfork Formations (Clardy and Bush, 1976). Both thrust faulting and the lithologic boundaries have an east-northeast trend, similar to the mercury deposit alignment (Figure 3). The spatial relationship of the mercury deposits to both regionally-mapped structural features and sandstone-shale contacts is fundamental in order to understand the importance of these potential controls to the depositional sites. The goal of this project was to determine which feature (fault traces or lithologic boundaries) better explains the linear depositional pattern of mercuric minerals within the region by examining which potential control mechanism is closer to the deposit locations. Presumably, the closer a controlling mechanism is to the site of deposition, the more influence it would have had on the deposit location. In order to accomplish this goal, the regional thrust faults and changes in lithology were mapped at an appropriate scale. A composite map of the changes in lithology, regional thrust faulting, and the deposits themselves were used to determine which of the suggested mechanisms exert more control on the placement of the deposits by being physically closer.

In order to accomplish these goals, a set of Geographic Information System (GIS) tools were utilized. GIS was used to map the regional thrust faulting, as well as the lithology. Regional thrust faulting in the area was mapped from the set of 1:24,000 geologic map quadrangles published by the Arkansas Geological Commission (2010) that cover the study

region shown in Figure 3. Sandstone and shale lithologies within the Stanley and Jackfork Formations had not been previously mapped separately, and required an alternative methodology to transferring location information from the existing geologic maps.

In order to map the lithologic changes, a methodology developed by Belt and Paxton (2005) was utilized, which investigated relationships between bedrock geology and changes in topography by using GIS. Their study utilized a 30-meter resolution Digital Elevation Model (DEM) and geologic map to visualize and quantify the relationships exhibited between the bedrock geology and topography in the north-central portion of Oklahoma. The study area consisted of weakly consolidated sandstone and shales, not unlike the area hosting the Arkansas mercury district. This methodology relies on the assumption that the weathering of these rocks has produced a differential topography between the two rock types. The study area exhibits a subtle, yet well-defined topography. Summaries of slope angle values and relief datasets, which were extracted from the DEM, were compared to the geologic formations present in the region. Findings by Belt and Paxton (2005) suggest that the local variations in topography in the region are strongly dependent on the abundance of sandstone and shale in the underlying bedrock. Sandstone, being more resistant to weathering, yields higher elevation areas and result in higher slope angles, while shale, being less resistant to weathering, yields lower elevation areas that result in lower slope angles.

Using this methodology and ArcGIS Desktop, a 5-meter resolution DEM was used to determine topographic attributes such as elevation and slope, as well as topographic wetness and plan curvature within the region of the Arkansas mercury district. ArcGIS 3D Analyst tools, such as “aspect” and “hillshade,” were used to aid in visualizing the topography so that the best investigation areas were selected. A composite map of these attributes was compiled using

ENVI 4.3, an image processing and analysis software. After a field visit, the investigation regions, one composed of more than 50% sandstone and one composed primarily of shale (50% sandstone abundance or less), were extracted from the composite maps using ENVI. Summary statistics from these investigation areas were extracted in order to determine the dominant elevation, slope, topographic wetness, and plan curvature characteristics for each of the rock types. User-defined sandstone and shale investigation regions, combined with the respective topographic attributes, such as elevation, slope, topographic wetness, and plan curvature were explored through the use of machine learning algorithms to evolve a set of relationship rules. The algorithm selected to evolve the relationships between topography and rock type is the decision learning algorithm C4.5 (Quinlan, 1993). These attributes were then used as input into the Waikato Environment for Knowledge Analysis (WEKA) software package, a data mining software containing multiple classifying algorithms, based on a user-defined set of positive and negative instances (Hall et al., 2009). The classifier, produced using the C4.5 algorithm, was used as a means to build a model to classify lithologies within the region. Application of this model created a thematic binary map of sandstone and shale within the region. Mapping of the regional lithologic changes was based on this map.

In order to determine which potential control mechanism (regional faulting or regional lithologic boundaries) better explains the position of the mercury deposition within the region, visual assessment and statistical analysis were performed on three datasets. These three datasets are composed of the distances found between each deposit and the nearest thrust fault and each deposit and the nearest lithologic change. The distances were systematically determined using the "near" tool in the ArcGIS Desktop suite. Summary statistics and a t-test were then computed to determine whether the two datasets were significantly different from one another. The dataset

with the smaller mean distance to the deposits is assumed to indicate the feature that best explains the depositional site and hence the alignment of mercury in the district.

CHAPTER 4. FIELD METHODS

4.1 Justification for Field Work

Field verification is fundamental in establishing the accuracy of this methodology, and was heavily focused on selecting the investigation regions (for both sandstone and shale) that were used to build the lithologic classification model. This verification is necessary because the model built for predicting the rock types within the region is based on these user-defined investigation regions. User-defined regions may be a source of error, and can be checked by comparison of the software-generated results to field observation.

4.2 Field Excursions

A trip to the study site was conducted on January 4-5, 2011 in order to investigate the regional variations in lithology, lithologic contacts, as well as regional topographic changes. The field observation sites selected for this study were based upon spatial location, ease of access, and outcrop visibility. Arkansas State Highway 27, a major north-south highway in the region, was selected for the majority of the field investigations. Highway 27 is the easiest to access and best maintained road within the region. This road was also beneficial because it crosses both regional lithologies (sandstone and shale) pertinent to this study. Various roadcuts along the north end of the study region along Highway 27 were investigated (Figure 5).

Areas adjacent to Lake Greeson were also investigated via hiking trails. Historic mercury mining operations were observed in the areas adjacent to Lake Greeson. Lithology type

elevation, and strike and dip of the ore bearing units were noted in the area. Ore bearing samples were observed along the abandoned test pits and waste stockpiles.

Each location was noted, either by hand on a topographic map or recorded using GPS. The length of rock exposure visible at each roadcut was estimated. The percent abundance of sandstone was estimated at each roadcut location.

In terms of lithologic composition, the Jackfork and Stanley Formations are very similar, in that they are both composed of sandstone and shale. Both formations are composed of sandstone interbedded with shale, or large shale units interbedded with sandstone. Both formations weather similarly in that that shale is less competent and weathers readily, yielding topographic lows; the opposite being true for the sandstone regions. Because of these similarities, field observations concerning lithology were made in terms of sandstone or shale (rather than Jackfork or Stanley Formations). Sandstone abundance was noted, rather than shale abundance, because the areas where an abundance of sandstone is present are more distinct because of the higher relief.

4.3 Field Observations

Each of the training regions needed for the mapping of the regional lithologic variations (via the model) were selected based on the results of the field observations made at each roadcut and at Lake Greeson. The sandstone training regions are comprised of more than 50% sandstone abundance. The shale training regions are comprised of less than 50% sandstone abundance.

It was evident from field observations, as well as on the topographic map of the region, that there is a distinct change in topography spanning from the north to the south of the region. Sandstone outcrops were readily available for field observations along Highway 27. Sandstone abundance was easiest to determine at these outcrops. There was an abrupt change in

topography, where the abundance of sandstone dropped significantly from approximately 50% abundance to much less, and thus the cutoff for sandstone and shale designation was made at 50% abundance.

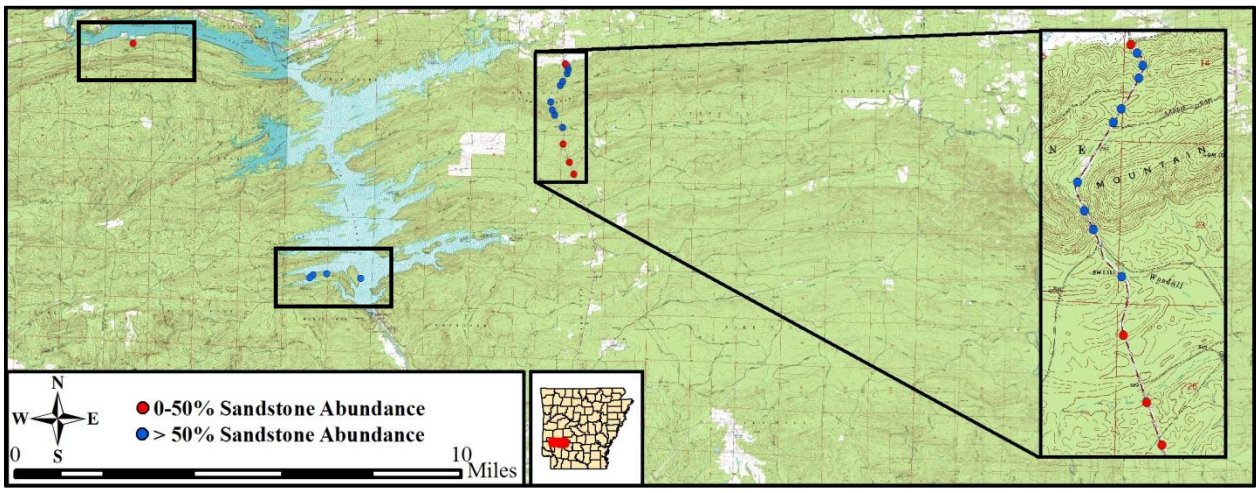

Figure 5.
Locations where observations were made and percent of sandstone abundance estimated at each site. The percent sandstone abundance at each roadcut along Highway 27 and adjacent to Lake Greeson are represented by red (50% sandstone abundance or less), and blue (greater than 50% sandstone abundance). The inset maps, outlined in black, highlight observations adjacent to Lake Greeson and along Highway 27.

4.4 Investigation Regions Derived from Field Work

The information collected from the field excursions were used to construct investigation data set polygons. A total of two types of investigation regions were drawn as polygons using ArcMap. These regions were comprised of sandstone (greater that 50% abundance present in the region), and shale (less than 50% sandstone abundance present in the region). Figure 6 depicts the two types of investigation regions drawn from the field data. The investigation regions, and topographic information extracted from these regions, were used in order to produce the machine-learned classifiers defined for the rock type classification model.

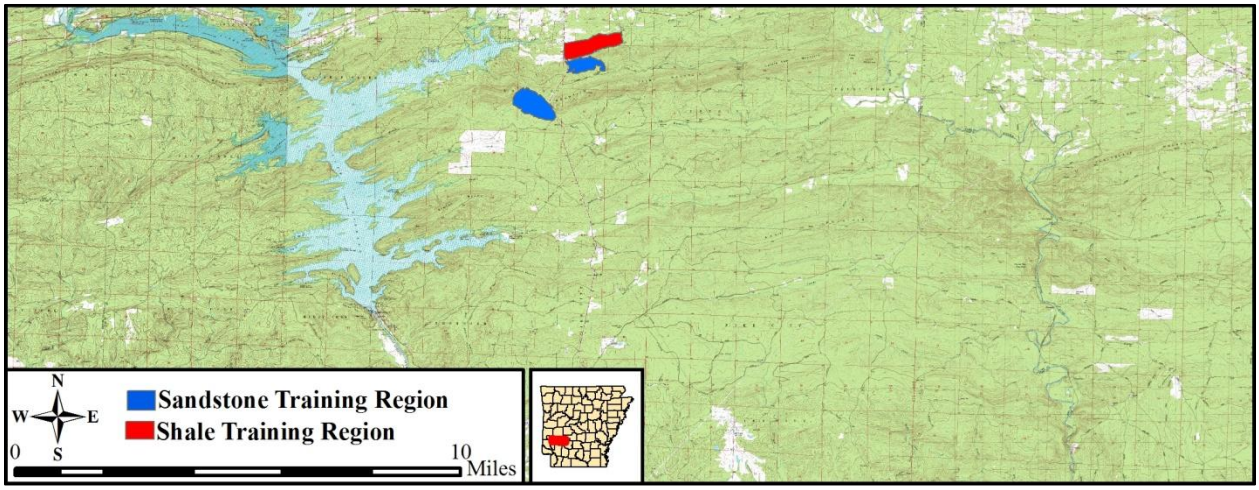

Figure 6.

The sandstone investigation regions are represented in blue and are comprised of more than 50% sandstone. The sandstone investigation regions consist of a total of 63,873 raster cells, where each cell is 5 meters by 5 meters. The shale investigation region is represented in red and is comprised of less than 50% sandstone abundance. The shale investigation region consists of a total of 44,711 raster cells, where 18 of which were removed because of no data values, resulting in 44,683 raster cells of the same 5-meter by 5-meter area.

CHAPTER 5. MODEL PARAMETERS

5.1 Topographic Attributes

Several topographic attributes served as parameters and the basis for building the rock type classification model for this project, specifically, elevation, slope, topographic wetness, and plan curvature. These topographic attributes, described below, serve as "predictors" for determining rock type within the model. These attributes are important because they all relate to weathering and geomorphological characteristics that differentiate the rock types. For example, sandstone, being a more competent rock than shale, is less readily weathered and will be more likely to have higher elevation values, steeper slope values, lower topographic wetness values, and a wider, more uniform range of plan curvature values. Conversely, shale, being a less competent rock than sandstone, weathers readily and will be more likely to have lower elevation values, lower slope values, higher topographic wetness vales, and a higher mean range of plan curvature values. Descriptions of each of the topographic attributes that served as model parameters for the rock type classification model (built from the decision tree classifier) are described below.

5.2 Digital Elevation Model (DEM)

The topographic attributes, used to build the rock type classification model for this project, were all derived from a 5-meter by 5-meter Digital Elevation Model (DEM) of the study area (Figure 7). The DEM used for this project was downloaded from the Arkansas Geographic Information Office (Arkansas State Land Information Board, 2007).

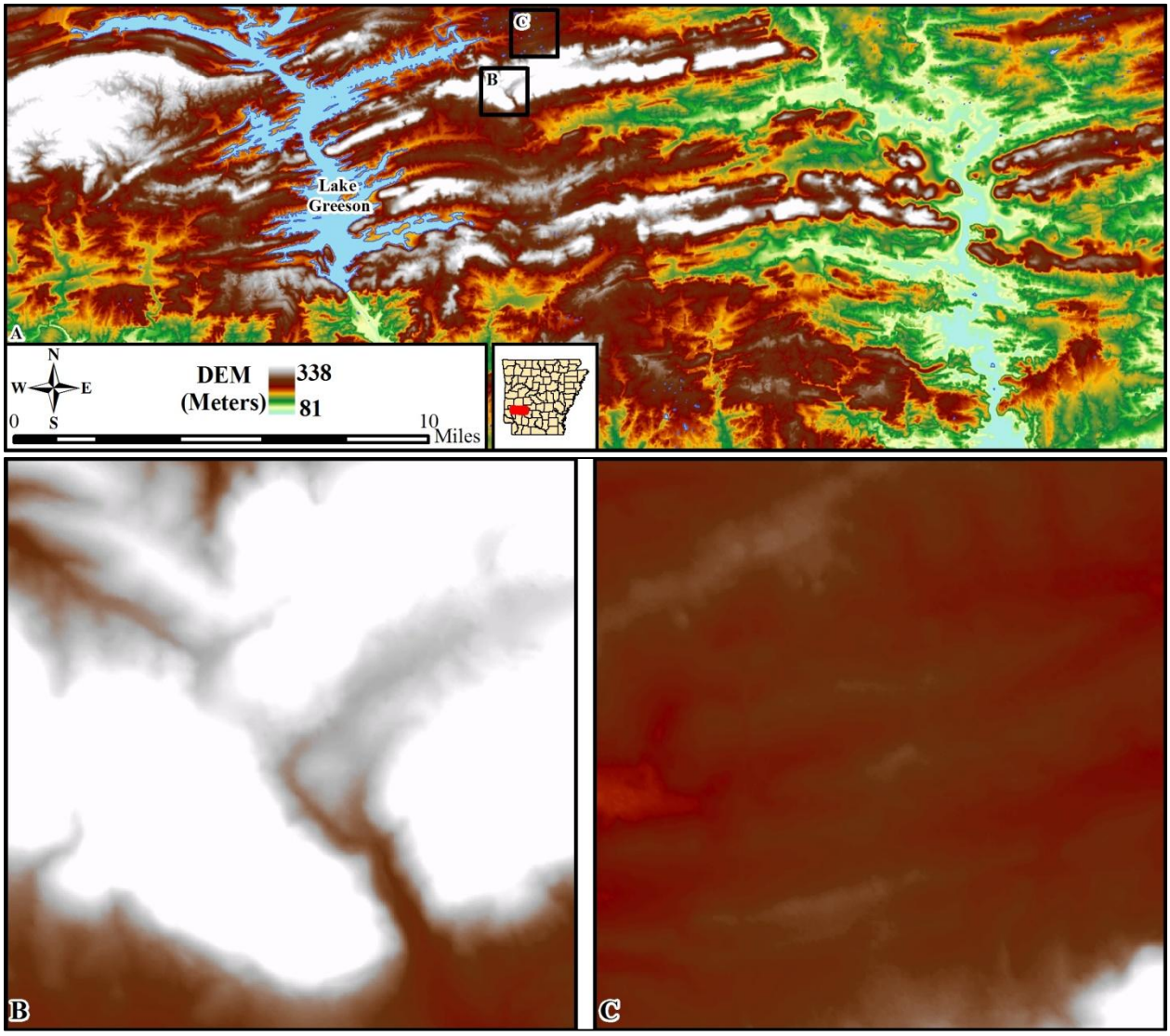

Figure 7.
Digital Elevation Model (DEM) acquired from the Arkansas Geographic Information Office (Arkansas State Land Information Board, 2007) for the entire region (Map 7A). The resolution is 5 meters by 5 meters. Shades of white to gray to brown represent higher elevations, while shades of yellow to green represent lower elevations. Shades of blue represent the lowest elevations found within the region. The elevations range from 81 meters above sea level to 338 meters above sea level. Map 7B (bottom left map) shows the sandstone region where investigation values were extracted. Note the abundance of higher elevation values. Map 7C (bottom right map) shows the shale investigation region. Note the abundance of low elevation values.

A DEM is a type of raster format which is composed of an ordered array of elevation values, spatially distributed across a region (Moore et al., 1991). These elevation values represent the topography of the Earth's surface. The DEM used for this project was produced via supplemental data collected from ortho-imagery acquired by the Leica ADS40 sensor (Arkansas State Land Information Board, 2007). From this DEM, four topographic attributes were derived (elevation, slope, topographic wetness, and plan curvature).

The elevation values, as well as several topographic indices of the area, were calculated using the DEM of the region. These values/indices serve as "attribute layers" for input to the decision tree learning model that was used to predict rock types within the district. Each attribute layer, described below, was extracted from each of the investigation regions (sandstone and shale), and compiled into a database for investigation using WEKA.

5.3 Topographic Attributes Derived from DEM

Combinations of primary and secondary topographic attributes were calculated in order to create the rock type classification model in this project. Primary topographic attributes, such as slope, aspect, and plan curvature, are attributes that are calculated or derived from directional derivatives of a topographic surface. A secondary topographic attribute, such as topographic wetness or stream power index, are computed from two or more primary attributes (Wilson and Gallant, 2001). The topographic attributes used for this project were elevation (taken directly from the DEM values), slope, topographic wetness, and plan curvature. These values are ideal because they vary over the spatial extent of the region, depending on rock type, and exhibit characteristic values that uniquely differentiate rock types within the region. These values vary because of the differing geomorphologic and weathering characteristics exhibited by each rock type.

Slope, a primary topographic attribute, is defined as the gradient found between two points (Wilson and Gallant, 2000). The slope function (θ), found in the 3-D analyst toolset of ArcGIS Desktop, calculates the rate of change (change in elevation, y, divided by the change in horizontal distance, x) between neighboring DEM cells. Slope is calculated:

$$\tan\theta = \frac{y_2 - y_1}{x_2 - x_1}$$

Results are output in degrees (ESRI, 2011). The significance of slope is related to overland and subsurface flow velocity and runoff rate, and geomorphology (Wilson and Gallant, 2000). Figure 8 shows the results of the slope values calculated from the 5-meter by 5-meter DEM.

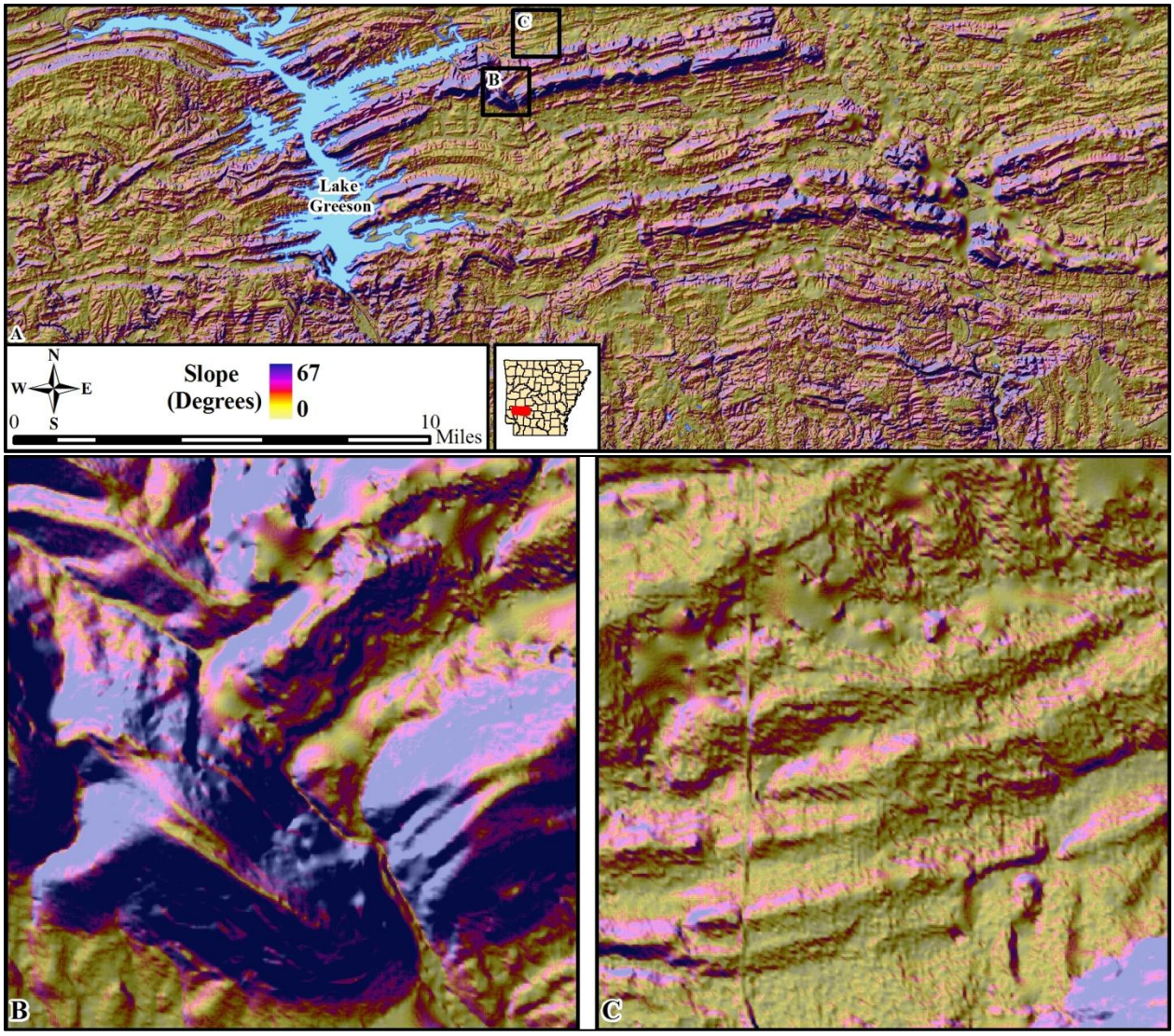

Figure 8.
Slope, in degrees, was calculated from the DEM (Figure 7) for the entire region (Map 8A). Higher slope values are represented by deepening shades of pink to purple, while lower slope gradients are represented by lightening shades of yellow. Slope values within the region range from 67 degrees to 0 degrees. Map 8B (bottom left map) shows the sandstone region where investigation values were extracted. Note the abundance of higher slope values. Map 8C (bottom right) shows the shale investigation region. Note the abundance of lower slope value.

Topographic wetness is a secondary topographic attribute, calculated from the DEM (Figure 7). Topographic wetness indices are used to describe the spatial distribution and extent of zones of saturation that may be the source for water runoff. The topographic wetness values calculated for this project are a function of the upslope contributing area, as well as slope gradient (Wilson and Gallant, 2000). Topographic wetness (*W*) is calculated:

$$W = \frac{A}{\tan B}$$

In this equation *A* is the area of a catchment basin (m^2), and *B* is the slope gradient in degrees (Moore et al., 1991). The highest values calculated in a topographic wetness index are typically found in the lowest areas of a catchment basin, suggesting the wettest points in the area (Wilson and Gallant, 2000). Alternately, the lowest values are found in higher elevations with the steepest slopes, and indicate less wet conditions. This relationship is assumed because water is more likely to drain from surfaces with high slope values. Figure 9 exhibits the topographic wetness values calculated within the region, shown as a map. A value of -1 indicates "no data."

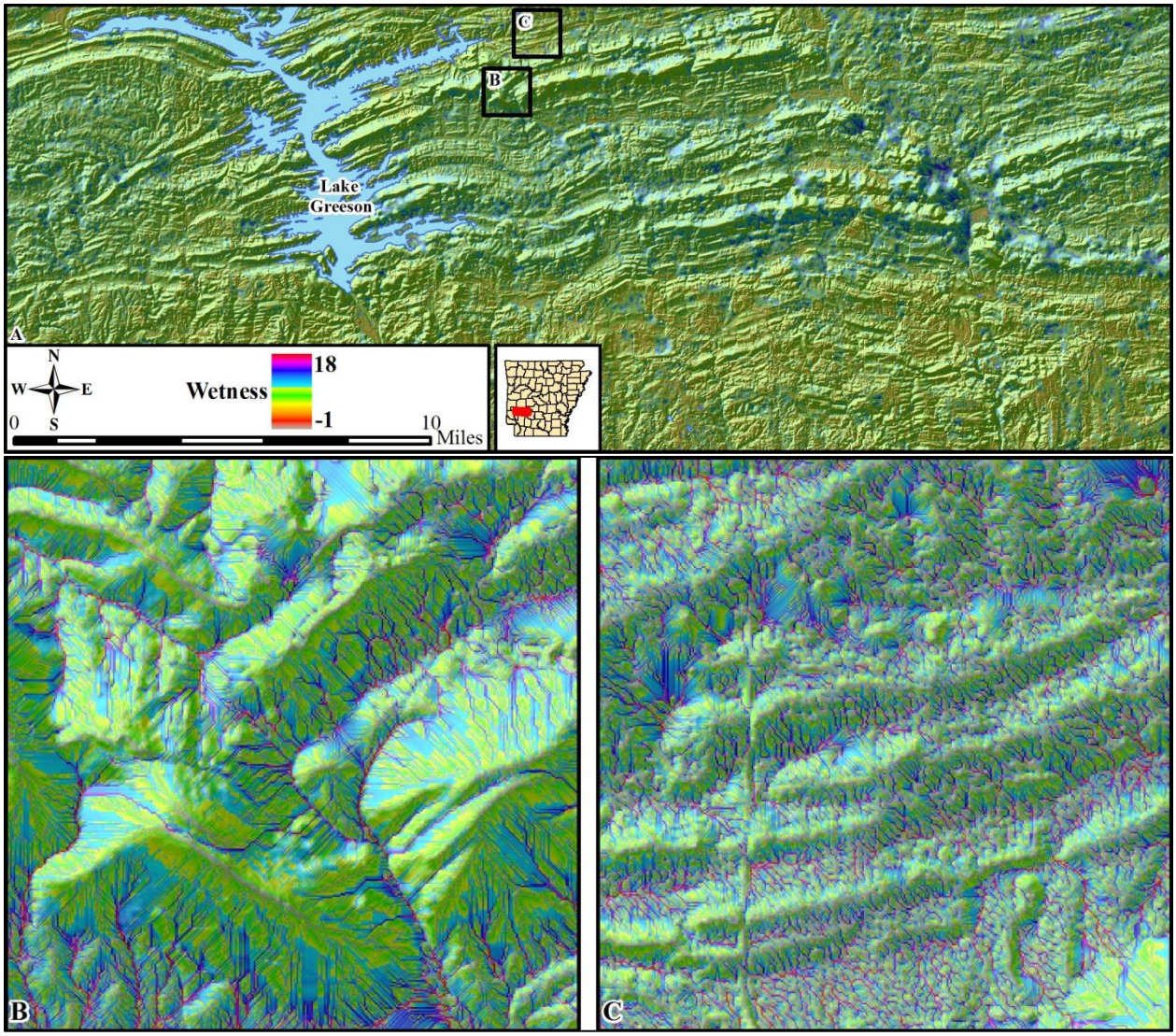

Figure 9.
Wetness values calculated from the DEM (Figure 7) for the entire region (Map 9A). Lower values are represented by shades of green to yellow and indicate higher regions with less wet points, while higher values are represented by varying shades of purple to blue, and indicate lower areas with the wettest points. Map 9B (bottom left map) shows the sandstone region where investigation values were extracted. Note the abundance of lower topographic wetness values. Map 9C (bottom right) shows the shale investigation region. Note the abundance of higher topographic wetness values.

The fourth topographic attribute used in the model created to classify rock type was plan curvature, also known as contour or planform curvature. Plan curvature is a primary topographic attribute, which is defined as the contour curvature over a region. Curvature is calculated from the second derivative of the rate of change of the derivative of the change in aspect (which is an azimuth value for the direction in which the slope face is directed) in a particular direction. Plan curvature is a measure of the convergence and divergence of topography, or the distribution of convex and concave surfaces. Plan curvature is the curvature of a line or contour in the horizontal direction and is reported in radians per 100 meters. Larger plan curvature values indicate tighter curves, while smaller plan curvature values indicate gentler curves. Plan curvature values are negative in areas with diverging flow characteristics, or on ridges. Conversely plan curvature values are positive in areas with converging flow characteristics, or in valleys (Wilson and Gallant, 2000). Values that are close to 0 indicate a relatively linear surface. Figure 10 exhibits plan curvature values calculated within the region, shown as a map.

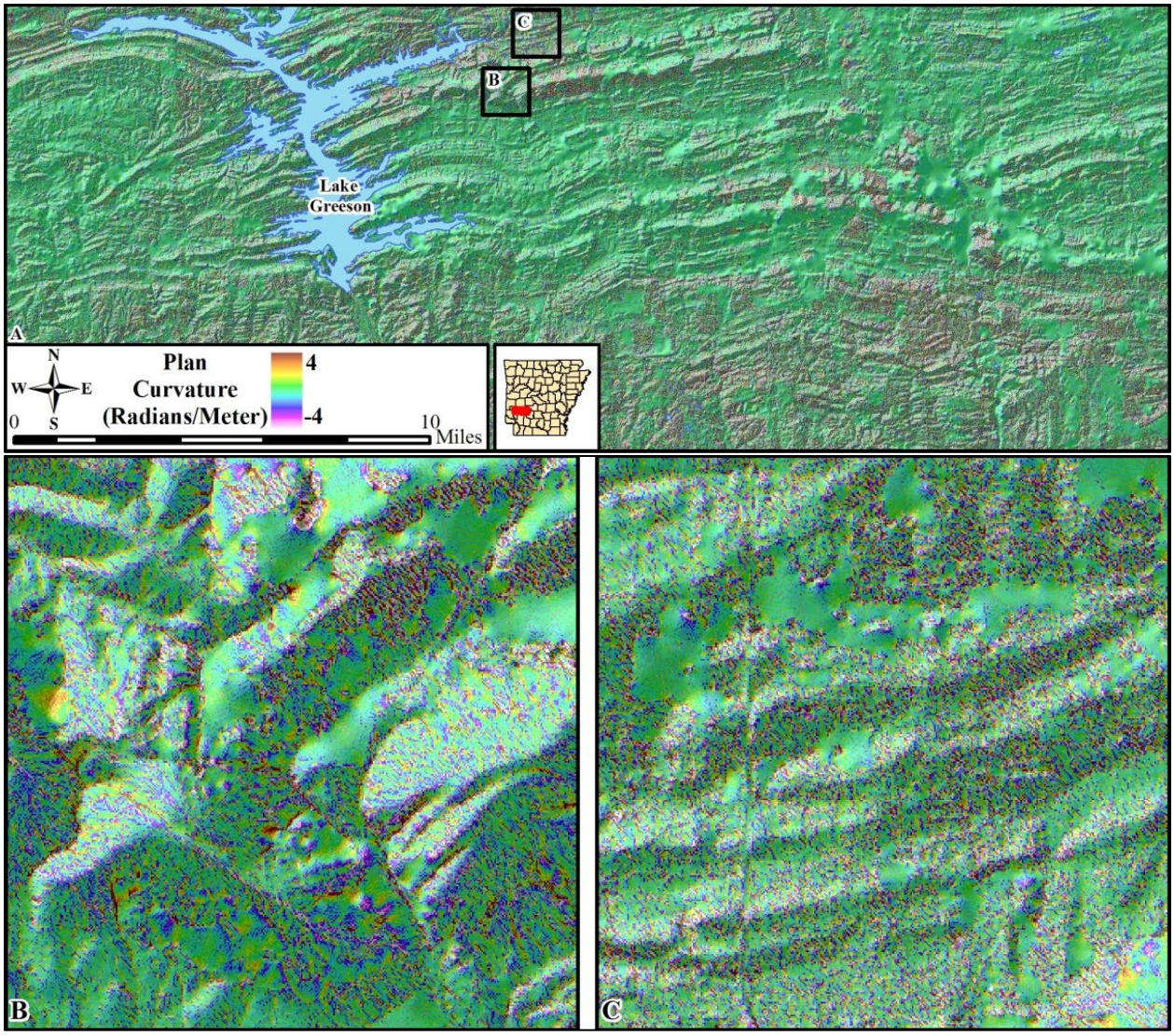

Figure 10.
Plan curvature values calculated from the DEM (Figure 7) for the entire region (Map 10A). High positive values (displayed in shades of yellow to brown) indicate converging areas found in valley regions. Low negative values (displayed in shades of blue to purple) indicated diverging flow areas typical of ridges. Shades of green represent median values of 0, indicating a relatively flat surface. Values within the region range from 4 to -4 radians per 100 meters. Map 10B (bottom left map) shows the sandstone region where investigation values were extracted. Note the abundance of lower plan curvature values, typical of ridges. Map 10C (bottom right) shows the shale investigation region. Note the abundance of higher plan curvature values, indicating valley regions.

CHAPTER 6. DATABASE INVESTIGATION

6.1 Database Construction

Once the training regions and topographic attributes were defined, data from the training regions were extracted. The values for elevation, slope, topographic wetness, and plan curvature were extracted from each cell of the raster within each training region using ENVI and compiled into a database.

There were a total of 63,873 sandstone entries and 44,711 shale entries. A total of 18 shale entries were removed because of "no data" values, totaling at 44,683. A "No data" value means that for that particular raster cell there was no topographic information provided for a particular attribute, rendering the raster cell unusable. Each entry represents a raster cell of the designated training region. For each raster cell, elevation, slope, topographic wetness, and plan curvature were determined.

6.2 Topographic Attribute Histograms

Histograms for each topographic attribute were compiled and investigated in order to ensure that each of the values were relatively unique enough to be used to create a model for rock type determination. A histogram is a graphical representation of the data distribution for a particular dataset. A histogram is created by plotting the range of data values (for a particular set) on the x-axis and plotting the number of occurrences (or frequency) of those dataset on the y-axis. The histograms for elevation, slope, topographic wetness, and plan curvature are shown as Figures 11, 12, 13, and 14. Characteristics for each rock type were uncovered through

observation of the histograms for each topographic attribute. A unique distribution of values was evident for the sandstone and shale investigation regions in Figures 11, 12, 13, and 14

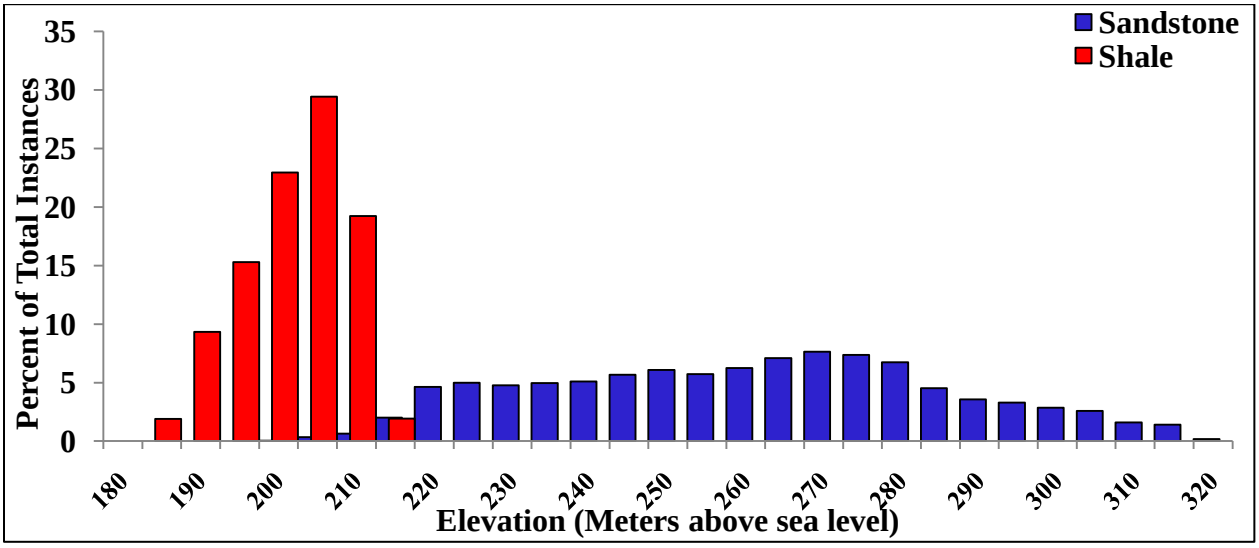

Figure 11.
Histogram representing elevations extracted from each lithologic investigation region. Sandstone is represented in blue and shale is represented in red. Note how both distributions vary greatly from one another, making elevation a useful attribute for modeling rock type.

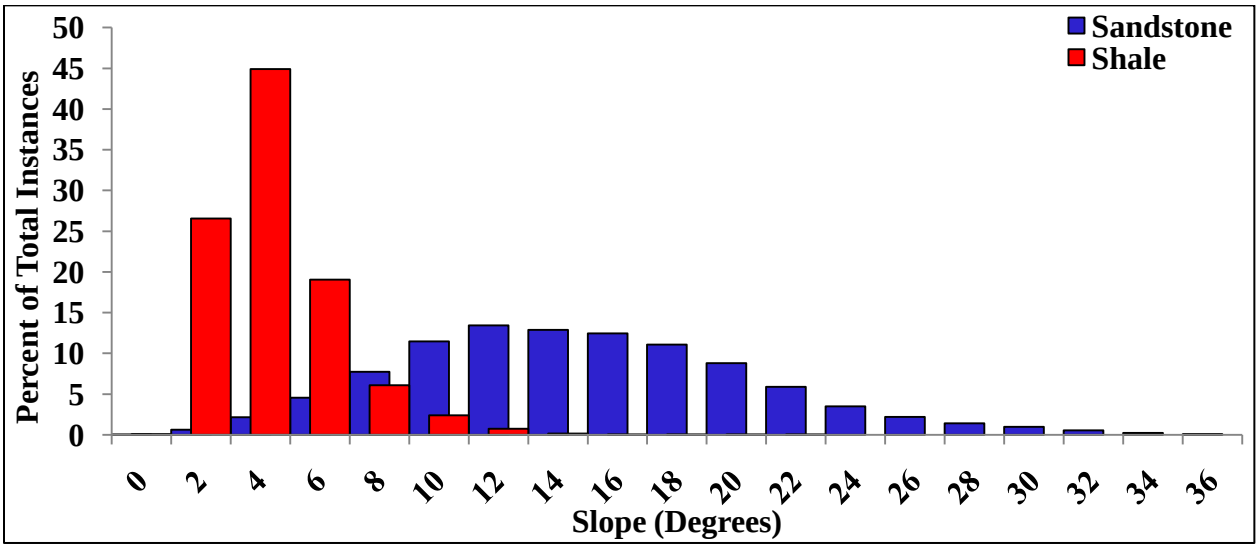

Figure 12.
Histogram representing slope values calculated within each lithologic investigation region. Sandstone is represented in blue and shale is represented in red. Note how both distributions vary greatly from one another, making slope a useful attribute for modeling rock type.

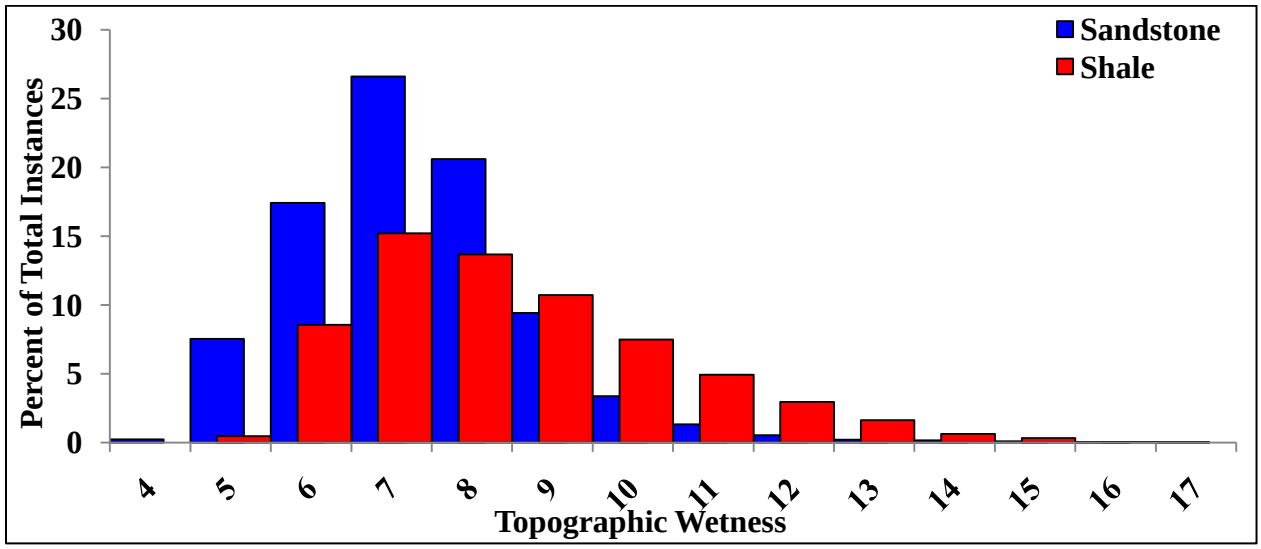

Figure 13.
Histogram representing topographic wetness values calculated within each lithologic investigation region. Sandstone is represented in blue and shale is represented in red. Note how the sandstone exhibits a lower mode value and the shale exhibits a higher mode value. Also, the shale shows a larger amount of high values, indicating topographic wetness is a useful attribute for modeling rock type.

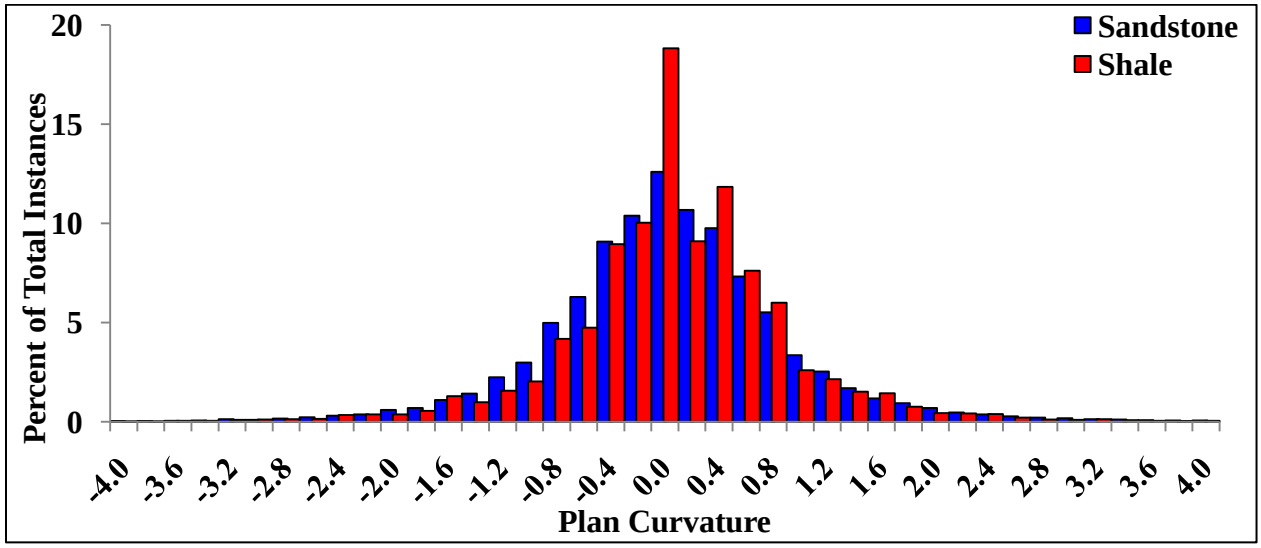

Figure 14.
Histograms representing plan curvature values calculated within each lithologic investigation region. Sandstone is represented in blue and shale is represented in red. Note how both histograms have a varying mode values, making plan curvature a unique attribute for modeling rock type.

Elevation values for the sandstone investigation regions ranged from 199 to 316 meters above sea level, while elevation values for the shale training region ranged from 182 to 213 meters above sea level. The elevation histogram (Figure 11) shows that the sandstone and shale lithologies have distinct elevation profiles, which is a result of differing erosion patterns for each rock type (Belt and Paxton, 2005). Because a distinct elevation profile exists for each rock type, elevation is an important prediction parameter for rock type classification.

The same type of relationship is evident for slope and rock type. Slope values for the sandstone investigation region ranged from 0° to 36°, while shale slope values ranged from 0° to 20°. The slope histogram (Figure 12) shows distinct distributions for the sandstone and shale slope values. Higher overall slope values for the sandstone region and lower overall slope values for the shale training regions are a result of differential weathering across varying rock types. Because this slope differential exists between rock types, slope is an important classifier of rock type. Overlap of values may also be indicating interbedding of the two rock types, where similar proportions of sandstone and shale are present.

Topographic wetness values for the sandstone investigation region ranged from 3.60 to 16.44, while the values within the shale investigation region ranged from 4.08 to 15.98. The topographic wetness histograms show distinct peaks for each of the rock types, sandstone and shale, within the region (Figure 13). Sandstone exhibits a lower mean value, at 6.81, while shale exhibits a higher mean value at 7.99. The shale histogram exhibits a skewed distribution to the right, toward higher topographic wetness values, relative to the sandstone histogram. Lower values indicate less wet areas, and topographically higher regions; while higher values indicate more wet areas, and topographically lower regions (Wilson and Gallant, 2000). For example, shale, being a less resistant (to weathering) rock type than sandstone, exhibits lower elevation

and relief values, lower slope angles, and higher overall topographic wetness values (because water is more likely to saturate in areas with these characteristics). Alternatively, sandstone is much more resistant to weathering than shale, which results in higher elevation values, higher slope values, and lower topographic wetness values (because water is more likely to runoff in areas with these characteristics). Topographic wetness values vary, depending on the erosional profile of the rock type in question. Because a distinct relationship between rock type and topographic wetness exists, topographic wetness is an important determinant for the rock type classifier.

Plan curvature values for the sandstone investigation region ranged from -10.64 to 9.11 radians/100 meters, while shale plan curvature values ranged from -5.52 to 6.37 radians/100 meters. The shale investigation region exhibits a narrower range of pan curvature values, implying that there is less variation of converging and diverging flow areas. Alternatively, the sandstone region exhibits a wider range of plan curvature values, implying that the surface is composed of more converging and diverging flow areas when compared to the shale (Wilson and Gallant, 2000). Areas with lower elevation and slope values, such as shale regions, are more likely to have less converging and diverging flow areas because the topography is not as abrupt when compared to a sandstone region that exhibits higher elevation and slope values. The shale region also shows a higher frequency of values at 0 (averaging at -0.003), implying that the surface is more linear or flat than the sandstone region. Because there is a fundamental relationship between topography and rock type, exhibited by plan curvature, it is a useful parameter for determining rock type.

6.3 Descriptive Statistics

Descriptive statistics were also calculated for each investigation region (sandstone and shale). Values are noted for each topographic attribute including: elevation, slope, topographic wetness, and plan curvature, as listed in Tables 1 and 2. Values that were calculated for each area (sandstone and shale) include: mean, standard error, median, mode, standard deviation, sample variance, kurtosis, skewness, range, and minimum and maximum value.

The mean of a dataset is defined as the sum of all of the entries divided by the total number of entries. The minimum value is the smallest data value within the dataset and the maximum value is the largest number in the dataset. The range of a dataset is simply the maximum minus the minimum. The mode is defined as the data value that repeats the most throughout a dataset when listed from minimum to maximum. The median value is defined as the value that occurs in the middle of a dataset. The variance of a dataset is the measure of the distribution of values around the mean value, and the square root of that value is known as the standard deviation. The standard error of a dataset is defined as the square root of the variance of a sample divided by the total number of instances in the dataset. The standard error describes the variation of the dataset (Davis, 2002).

Note the differences between the mean values for the sandstone and shale investigation regions. Large differences in values are ideal for investigation regions that are going to be used to build a decision tree classifier. The sandstone investigation region has a mean elevation of 258 meters, whereas the shale investigation region mean elevation is 199 meters above sea level. The mean slope value for the sandstone region is 14°, whereas the mean shale slope value was 3°. The mean topographic wetness value for the sandstone investigation region was found to be 6.81, whereas the mean for the shale region was 7.99. Plan curvature values also varied from

-0.04 for the sandstone to -0.003 for the shale region.

SANDSTONE DESCRIPTIVE STATISTICS				
	Elevation (Meters)	**Slope (Degrees)**	**Topographic Wetness**	**Plan Curvature (radians/100 meters)**
Mean	258	14	6.81	-0.04
Standard Error	0.10	0.02	0.01	0.003
Median	259	14	6.72	-0.03
Mode	279	9	6.21	0
Standard Deviation	25.6	5.8	1.42	0.94
Sample Variance	655.8	34.02	2.03	0.89
Kurtosis	-0.8	0.08	2.10	5.88
Skewness	0.1	0.43	0.88	0.34
Range	117	36	12.84	19.75
Minimum	199	0	3.60	-10.64
Maximum	316	36	16.44	9.11

Table 1.
Descriptive statistics calculated for the sandstone training region dataset.

SHALE DESCRIPTIVE STATISTICS				
	Elevation (Meters)	**Slope (Degrees)**	**Topographic Wetness**	**Plan Curvature (radians/100 meters)**
Mean	199	3	7.99	-0.003
Standard Error	0.03	0.01	0.01	0.004
Median	200	3	7.64	0
Mode	204	3	6.21	0
Standard Deviation	6.6	1.99	1.92	0.82
Sample Variance	43.4	3.96	3.68	0.67
Kurtosis	-0.6	2.83	0.31	3.45
Skewness	-0.4	1.36	0.82	0.04
Range	31	20	11.90	11.89
Minimum	182	0	4.08	-5.52
Maximum	213	20	15.98	6.37

Table 2.
Descriptive statistics calculated for the shale training region dataset.

CHAPTER 7. DECISION TREE CLASSIFICATION MODEL

The investigation regions and subsequent data values collected from the field portion of this project were investigated using the WEKA software in order to determine a set of rule classifiers outlined by a decision tree. The WEKA software utilized the J48 Java implementation of the C4.5 machine learning algorithm to train and test each rock type investigation region and output a set of rule classifiers in the form of a decision tree. This process takes the investigation regions (sandstone and shale) and divides them into training subsets and testing subsets. The training subset, approximately one-third of the investigation region dataset, is used to build the decision tree, while the remaining testing subset, approximately two-thirds of the investigation region dataset, is used to test the model that was created using the training subset.

Decision tree learning is a computer-based searching method which attempts to approximate discrete-values in order to "learn" a known function. The output of a decision tree can be represented as set of if-then statements that may be used in order to define the known function. The advantage of using a decision tree learning method is that the outputs of if-then statements are easily interpreted by humans (Mitchell, 1997).

A decision tree works by attempting to classify instances by sorting them down a "tree." A decision tree is made up of "leaf nodes," which classify each instance (for this project the instances are either sandstone or shale). Every node of the tree tests a specific attribute (in this case there are four attributes: elevation, slope, topographic wetness, and plan curvature). The branches of the nodes are made up of possible corresponding values for the attribute associated

with that node (Mitchell, 1997). Figure 15 is a simplified example of the decision tree produced for this project.

The decision tree works by using the C4.5 algorithm to determine a top to bottom decision process that begins with the attribute that is best suited for the "root" or the first question in the tree. For each instance an attribute is evaluated using statistical analysis to determine how well each attribute classifies each instance alone. The attribute that classifies most of the instances alone is used as the root of the tree, or the first decision. For this model, elevation was determined as the root of the tree because for the majority of sandstone and shale instances, elevation alone classified the instance correctly. Descendants of the root node are then determined for every possible attribute value and the resulting training values are sorted accordingly down the tree. This process is repeated at each descendant node to select the next best attribute for testing that point in the tree (Mitchell, 1997). Selecting the best attribute for classifying each node in the tree is done by determining the information gain of a particular attribute. Information gain is a statistical property that measures how well a particular attribute is able to separate instances according to their classification. The information gain measure is used to select the best attributes for each step while expanding the tree (Mitchell, 1997).

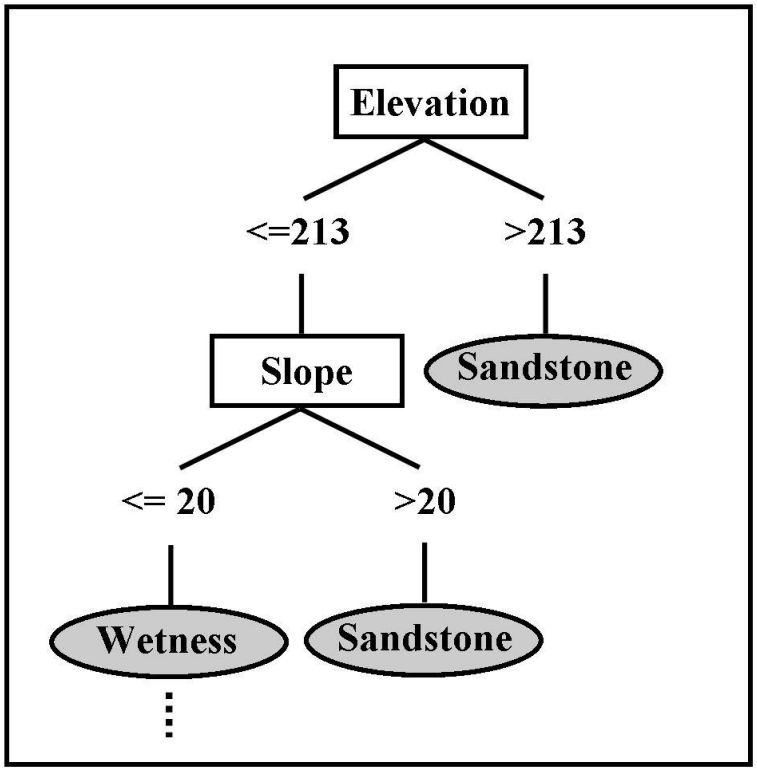

Figure 15.
Simplified excerpt of the decision tree produced for this project. Note that if the elevation node value lies above 213 then the instance is classified as sandstone. If the elevation value is less than or equal to 213 then the slope subnode is followed. If the slope value is greater than 20 the instance is classified as sandstone.

CHAPTER 8. DECISION TREE CLASSIFICATION MODEL RESULTS

8.1 Decision Tree Classification Results: WEKA

After the investigation region database compilation was completed, WEKA was implemented in order to build the rock type classification model. The J48 decision-learning algorithm was applied to the database. Of the total 108,566 investigation region database entries, approximately one-third (35,827 sandstone and shale instances) were used to train (build the model) and the remaining two-thirds (72,739 sandstone and shale instances) were used to test the model. The final model used for rock type classification was output in decision tree form and is displayed in Appendix 1. The final decision tree was comprised of 68 leaves and a total of size of 135 nodes.

Summaries concerning the accuracy of the decision tree classifier on the testing subset are listed in Table 3. Values were calculated for correctly and incorrectly classified instances, and the Kappa statistic. These values are important in understanding how the error attained during the classification process varies.

The Kappa statistic (listed in Table 3) is a number that measures the accuracy of a confusion matrix (Table 4), which is a listing of the correct and incorrect classifications. The Kappa statistic summarizes the confusion matrix by combining the observed agreement, and the chance of random agreement of the variables. Not every case of agreement achieved during the classification process is attributable to success of the process, because some of the cases may agree based on chance. For this reason, the Kappa statistic takes into account both factors. The

Kappa statistic ranges from 0 to 1, where a Kappa statistic of 1 indicates a perfect classification scheme, or no random agreement. The Kappa statistic is different from overall accuracy in that overall accuracy does not take into account the chance for random agreement (Aronoff, 2005).

Out of a total of 72,739 testing subset instances, the decision tree classifier (built using the training subset of 35,827 instances) output 99.5% correctly classified test subset instances, or 72,408 instances, and only 0.5% were incorrectly classified, or 331 test subset instances. The Kappa statistic for the decision tree classifier was 0.9906. The results of the classification activities of the decision tree classifier on the testing subset are summarized in Tables 3, 4 and 5.

Summary Results of Classification of Testing Subset		
Correctly Classified Instances	72408	99.5%
Incorrectly Classified Instances	331	0.5%
Kappa statistic	0.9906	
Total Number of Instances	72739	

Table 3.
Summary of classification results of the decision tree classifier. Results pertain only to testing subset instances that were classified according to the decision tree classifier.

A confusion matrix for the classification results was also calculated (Table 4). The results of the confusion matrix show that 42,560 testing subset sandstone instances were correctly classified as sandstone, while 268 of the testing subset sandstone instances were misclassified as shale. The matrix also shows that 29,848 shale instances were correctly classified as shale, while 63 of the shale instances were misclassified as sandstone.

Confusion Matrix for Classification Results on Testing Subset			
	Classified as Sandstone	Classified as Shale	Total Classified
Sandstone Instance	42560	268	42828
Shale Instance	63	29848	29911
Total Instances	42623	30116	72739

Table 4.
Confusion matrix for the decision tree classification system built from the sandstone and shale training subset. Results pertain only to testing subset instances that were classified according to the decision tree classifier.

The detailed accuracy by class report (Table 5) summarizes classification results of the decision tree classifier on the testing subset. The True Positive (TP) Rate, False Positive (FP) Rate, Precision, Recall, and F-measure are given for each class as well as the weighted average of both classes. These values are important in understanding how the classification scheme performed. High TP Rates, Precision, Recall, and F-Measure scores (out of 1.000), and low FP Rates (out of 1.000) indicate high accuracy in performing the classification procedure on the testing subset. These values were calculated from the confusion matrix in Table 4.

The TP and FP rates are important because they provide insight on performance of the classification schema (decision tree) developed using the training subset. The TP rate is defined as the number of sandstone or shale instances that were correctly classified in the testing subset as sandstone or shale divided by the total number of known sandstone or shale instances in the testing subset. For example, there were a total of 42,560 correctly classified sandstone instances out of a total of 42,828 sandstone instances, giving a TP rate of 0.994 for the sandstone. Conversely, the FP rate is defined as the number of sandstone or shale instances that were misclassified in the testing subset as sandstone or shale divided by the total number of sandstone or shale instances in the testing subset. For example, there were a total of 63 shale instances that were misclassified as sandstone. The number of misclassified shale instances (63) divided by the total number of shale instances (29,911) equals an FP rate of 0.002 for the sandstone (Sokolova et al., 2006).

The precision is defined as the number of true positives divided by the sum of the true positives and the false positives. For example, the number of true positives for sandstone testing subset was 42,560, while the number of false positives was 63 (Table 4). The number of true positives (42,560) divided by the sum of the true positives (42,560) and false positives (63)

equals a precision of 0.999 (Table 5). The recall is defined as the ratio of the number of true positives divided by the total number of classified instances. For example, there were a total of 42,560 correctly classified sandstone instances and a total of 42,828 sandstone testing instances (Table 4), giving a recall of 0.994 (Sokolova et al., 2006; Makhoul et al., 1999). In essence, the recall is the same as the true positive rate. The F-measure is defined as the weighted average of precision and recall (Makhoul et al., 1999).

The weighted averages of the TP and FP rates were 0.995 and 0.004, respectively. The weighted average of the precision for both classes was 0.995. The weighted average of the recall for both classes was 0.995. The weighted average of the F-measure for both classifications was 0.995.

Detailed Accuracy By Class for Testing Subset					
Class	TP Rate	FP Rate	Precision	Recall	F-Measure
Sandstone	0.994	0.002	0.999	0.994	0.996
Shale	0.998	0.006	0.991	0.998	0.994
Weighted Avg.	0.995	0.004	0.995	0.995	0.995

Table 5.
Accuracy results of the decision tree classifier on sandstone and shale testing subset. The True Positive (TP) rate, False Positive (FP) rate, precision, recall, and F-measure, are summarized by class and the weighted average for both classes.

Because the summary reports for the decision tree classification scheme using elevation, slope, topographic wetness, and plan curvature as predicting attributes reported numbers that imply high accuracy, this decision tree classification scheme was chosen for use as the rock type classification model for the region.

8.2 Rock Type Classification Model Results

The decision tree classifier, output by WEKA, was used as the rock type classification model for this project. The rock type classification model was applied to a raster of the entire study region (Figure 3) in an automated fashion. The resulting sandstone and shale classification is shown in Figure 16. The areas shaded blue were classified as sandstone, while the area shaded gray are classified as shale.

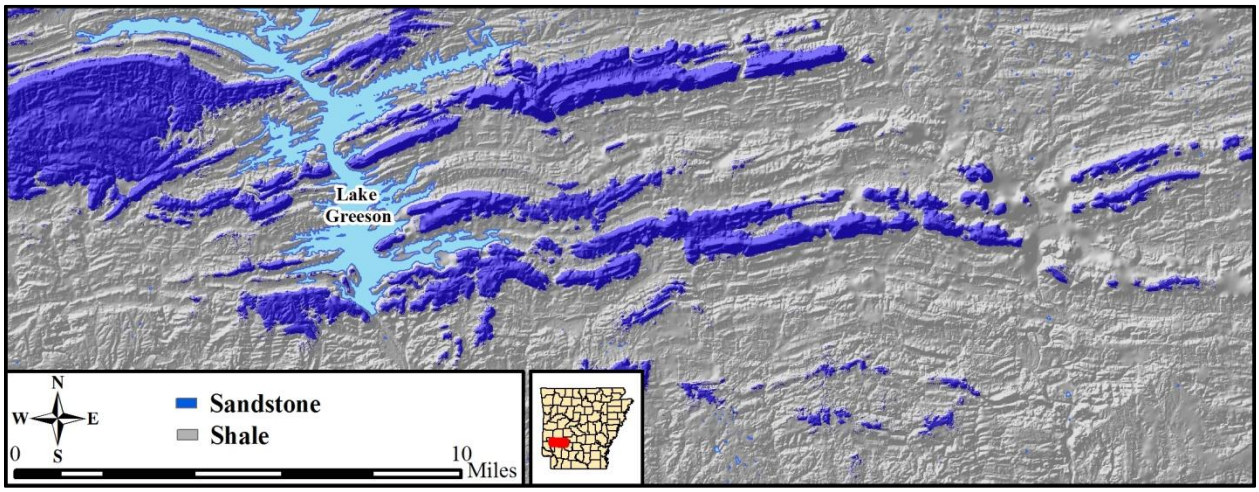

Figure 16.
Final rock type classification model results, as applied to the region. Areas shaded blue represent areas classified as sandstone. The areas shaded gray represent shale.

8.3 Discussion of Model Results

The rock type classification model results were visually compared to the field observations discussed in Chapter 4 (Figure 17). The areas shaded blue represent sandstone in the model, while areas shaded gray represent shale regions. Field observations are represented as red or yellow dots. Red dots indicate field observations that are less than 50% sandstone abundance, while yellow dots indicate field observations of more than 50% sandstone abundance.

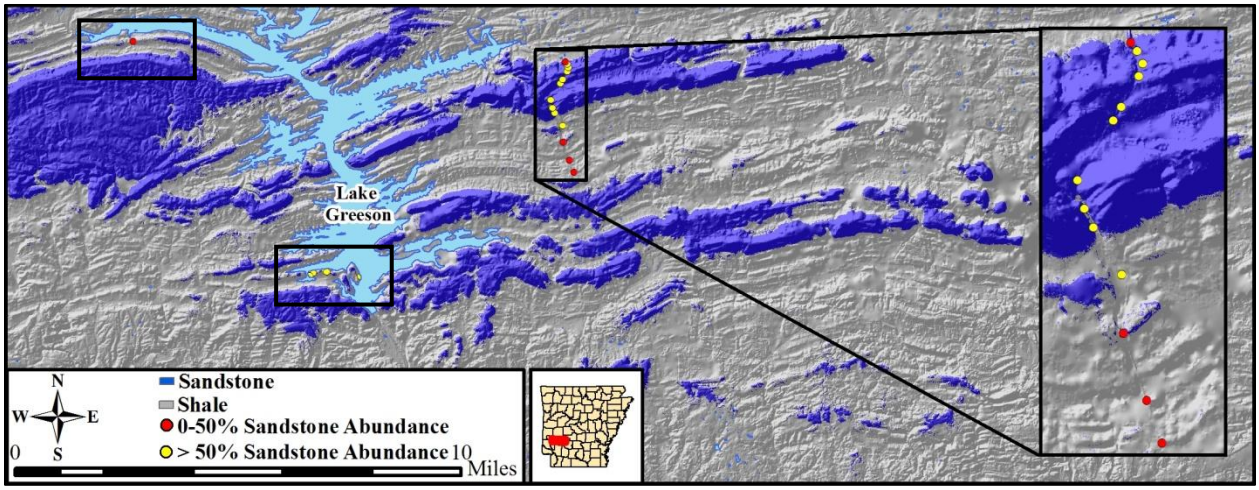

Figure 17.
Visual comparison of the rock type classification results and field observation. Observations represented by red dots indicate a sandstone abundance of 0 to 50%. Observations represented by yellow dots indicate sandstone abundance of greater than 50%.

The rock type classification model, when compared to field observations, identified the majority of known sandstone regions from the topographic attribute information used in the decision tree. Visual comparison of the geologic map of the region (Figure 18) shows that most of the classified sandstone was within the Jackfork Formation, agreeing with regional geology.

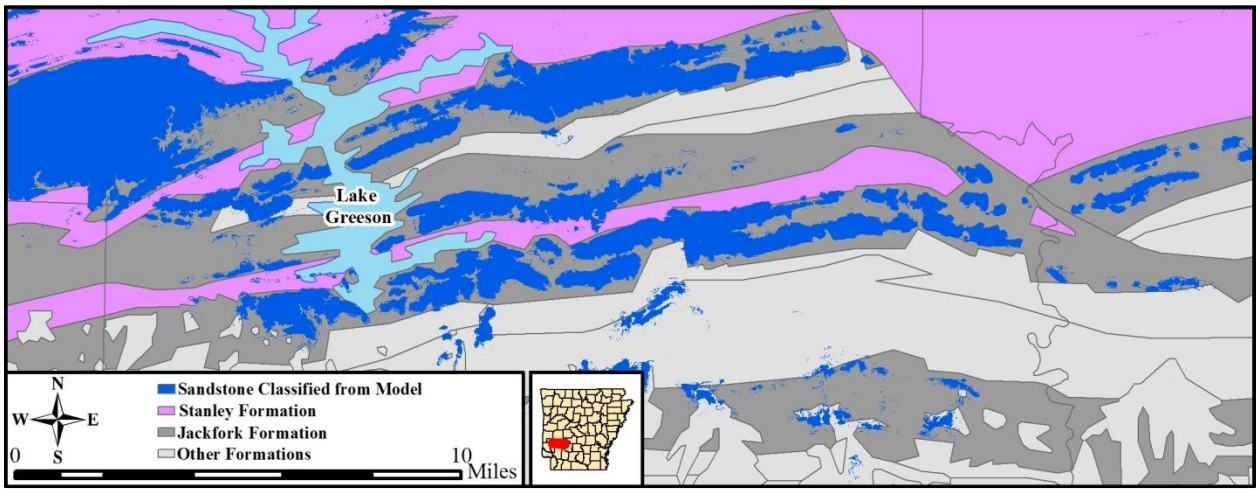

Figure 18.
Visual comparison of the rock type classification results (shown in blue) and the geologic map of the region. The Stanley Formation is represented in pink and the Jackfork Formation is represented in dark gray. All other formations are shown in light gray.

Reasons for this could be due do varying thicknesses of individual sandstone layers. For example, the Stanley Formation has thinner intervals of interbedded sandstone than the Jackfork Formation and therefore has a differing weathering profile (lower relief due to an overall less resistant package of rocks). The Stanley Formation is composed of thicker shale intervals than the Jackfork Formation. Other reasons for this could be attributed to the investigation regions selected for this project. The investigation regions selected for this project occupied predominantly the northern section of the study area where elevation values for the sandstone are higher and occupy mostly the Jackfork Formation. The elevation attribute used in this model is very important because it is one of the first classifier used to determine rock type. The topographic values used to classify the sandstone were extracted from the northern portion of the map, where sandstone elevations are overall higher. This may have affected the ability of the model to classify sandstones in the southern portion of the region. The Stanley Formation sandstones, which host the mercury mineralization, are south of the training regions and at a lower elevation.

The rock type classification model did properly classify some of the Stanley Formation sandstones; however, they were mostly on the west side of Lake Greeson. Almost none of the Stanley Formation sandstones were classified on the east side of the lake (Figure 18). The rock type classification model classified the majority of sandstones that dominate the Jackfork Formation; however, in the extreme southwest side of the region the model did not classify the Jackfork Sandstones (Figure 18).

CHAPTER 9. FINAL MAPS

9.1 Mapping of Mercury Deposits, Faulting, and Sandstone

Mapping of the faults and mercury deposits within the region were completed using the 1:24,000 scale geologic maps of the region as a base. Geologic maps were downloaded from the Arkansas Geologic Commission (2010) website and were imported into ArcGIS Desktop. Geologic map references are shown in Appendix 2. The maps were then converted to a useable format, georeferenced, clipped, and the faults were digitized. The faults were digitized by hand using the ArcGIS "Draw" tool. The final map of the faults and mercury deposits in the study area are shown as Figure 19.

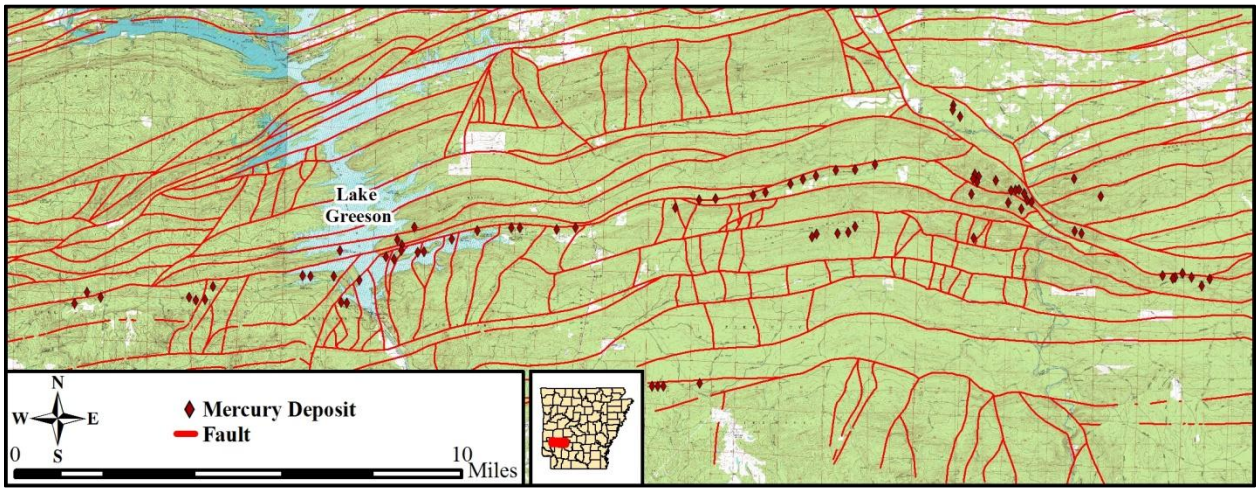

Figure 19.
Faults (red lines) displayed over the 1:24,000 topographic map of the region. Mercury deposits are shown as red diamonds.

The final raster output of the rock type classification model discussed previously was used as the basis to map the sandstone units within the region. Once again, the ArcGIS Desktop suite was used to aid in the mapping of the region. First, the raster output of the model was converted into a useable format for the distance measuring portion of the project described in Chapter 10. Figure 20 shows the final map output of the sandstone mapping, as well as the faults and mercury deposits within the Arkansas mercury district.

9.2 Composite Map

Once final maps of the sandstone units, mercury deposits, and faults were completed for the entire region, they were compiled using ArcGIS and displayed (Figure 20). The composite map was necessary in order to complete the next phase of the project, which was to measure and analyze the distances found between each deposit and the closest sandstone-shale contact, as well as each deposit and the closest fault within the region.

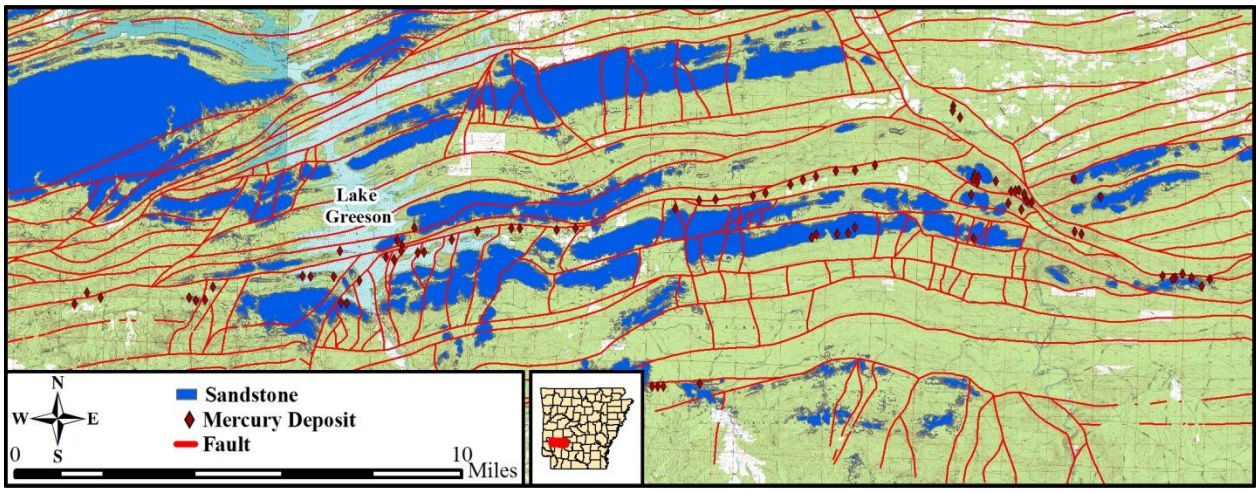

Figure 20.
Final composite map of the sandstone outcrops (blue), mercury deposits (red diamonds), and faults (red lines) within the Arkansas mercury district.

CHAPTER 10- DATA ANALYSIS

10.1 Measuring Distances

Once the composite maps were complete, the ArcGIS Desktop "Near" tool was used to measure the nearest straight line distance between each deposit and the nearest sandstone-shale contact, as well as the nearest fault surface trace. Figure 21 shows how the distance is measured using the "Near" tool. Results are output in meters (ESRI, 2011).

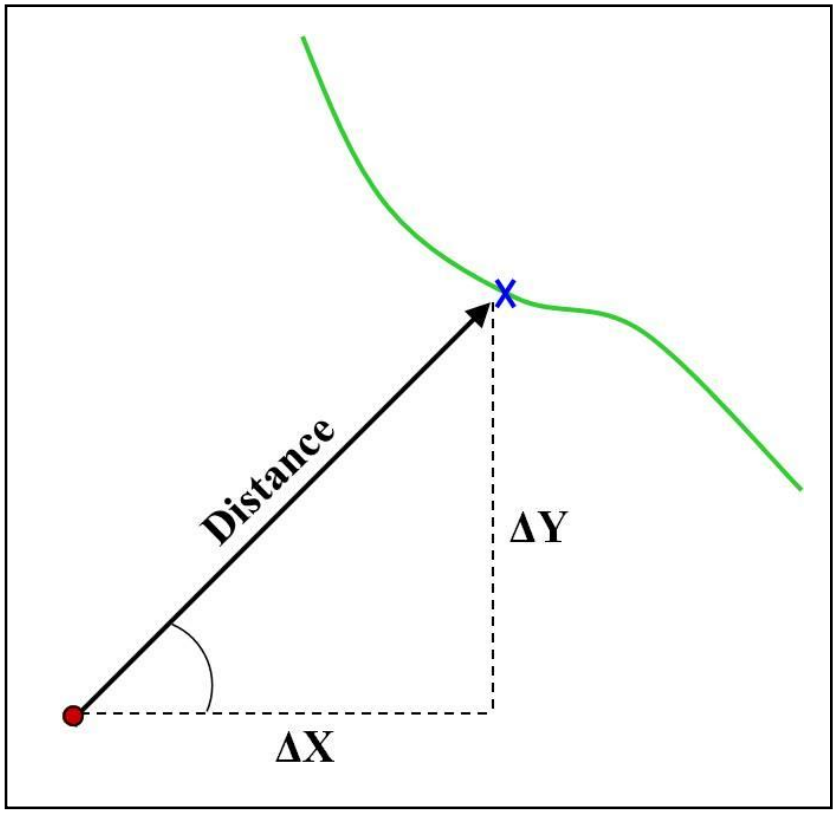

Figure 21.
Example of how the "Near" tool measures distance between deposit (red dot) and fault/contact (green line or blue "X") (Figure modified from ArcGIS Desktop (ESRI, 2011)).

10.2 Result analysis

In order to analyze the distance data, a database of the distance measured for each deposit location was configured. Appendix 3 lists 77 deposits, their location and elevation, and the straight line distance between each deposit and the nearest fault and the nearest contact. Figure 22 is a graphical representation of the distances measured. The deposits were number from west to east in numerical order. Groups of deposits that were found to be outside of the alignment of the majority of the deposits were also numbered in this fashion. A total of 41 deposits were determined to be closer to a contact, while the remaining 36 deposits are closer to a fault.

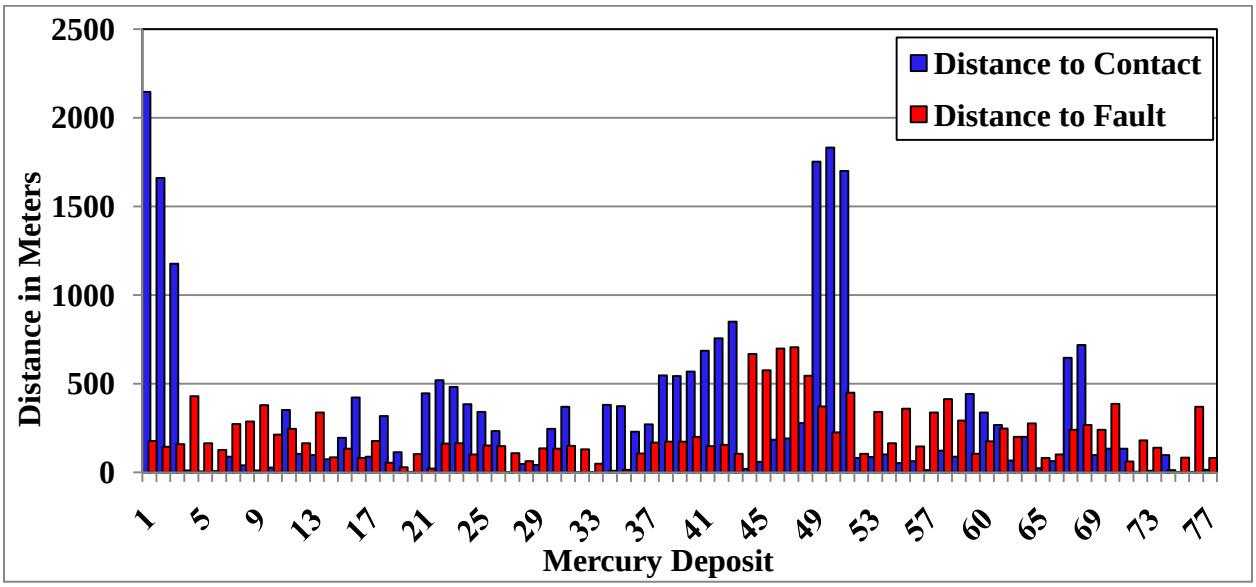

Figure 22.
Comparison of distances between each deposit and the nearest sandstone-shale contact (blue) and each deposit and the nearest fault (red).

Summary statistics (Tables 6 and 7) were computed for distances measured between each deposit and the closest fault, as well as distances measured between each deposit and the closest contact. The mean distance from a deposit to a fault was 211 meters. The mean distance from a deposit to a contact was 327 meters.

Fault Summary Statistics	
Mean	211
Standard Error	18
Median	164
Standard Deviation	155
Sample Variance	24160
Kurtosis	2
Skewness	1
Range	696
Minimum	10
Maximum	706

Table 6.
Summary statistics computed for distances found between mercury deposits and closest faults.

Contact Summary Statistics	
Mean	327
Standard Error	53
Median	134
Standard Deviation	463
Sample Variance	214429
Kurtosis	6
Skewness	2
Range	2147
Minimum	0
Maximum	2147

Table 7.
Summary statistics computed for distances found between mercury deposits and closest sandstone-shale contact.

CHAPTER 11. DISCUSSION

11.1 Result interpretation

T-tests were conducted on the datasets previously discussed. The t-test investigated distances between deposits and faults and deposits and sandstone-shale contacts (Table 8). The t-test that was conducted assumed two samples (distance between deposits and faults and deposits and contacts) with no difference between means. The alpha value (or the significance/confidence level) chosen for this test was 0.04. The null hypothesis for this test was that there is no difference between the means of the distances, or a difference of 0.

The t-test was chosen to analyze the distance measurement results because it is useful for comparing two population samples at one time. The null hypotheses for these tests assume that there is no difference between the means of the two datasets. The p-value for this test, or the observed significance level, is defined as the probability that the t-statistic calculated is indeed contradictory to the null hypothesis (in this case that there is no difference between the means in the datasets). If the p-statistic is smaller than the significance level (0.04) chosen for the test, then the null hypothesis is rejected (Devore and Farnum, 1999).

t-Test: Paired Two Sample for Means		
	Distance to Fault	***Distance to Contact***
Mean	211	327
Variance	24160	214429
Observations	77	77
Hypothesized Mean Difference	0	
Df	76	
t Stat	-2.097	
P(T<=t) one-tail	0.020	
t Critical two-tail	2.090	

Table 8.
T-test between the distances calculated from each mercury deposit to the closest fault and the closest contact.

Results from the t-tests performed for this project conclude that both of the means for both datasets are statistically significantly different from one another. The t critical statistic for this t-test was 2.090 and the calculated t statistic, for the 96% confidence level, was found to be -2.097. Because the absolute value of the t statistic is larger than the t critical two-tail statistic (2.090), the null hypothesis is rejected at a 96% confidence level (Davis, 2002). The mean of the fault distances and the mean of the contact distances are statistically different. Because the t statistic is negative, it implies that the fault distances are the smaller of the two averages and thus the more likely to have influenced the deposit location.

Although the distance analysis showed that there were 41 deposits found to be closer to a sandstone-shale contact and 36 deposits found to be closer to a fault, the results of the t-test suggest that the faulting is the more controlling feature in determining the deposit location. This apparently contradictory result could be due to the presence of regional variations as well as errors in mapping the sandstone. For example, under-classification of sandstone would result in fewer deposits located within the sandstone regions or near a sandstone-shale contact.

11.2 Regional variations

The results of the distance analysis were also visually compared for regional variations. Figure 23 shows deposits that are closer to sandstone-shale contacts (blue) and deposits that are closer to faults (red). Visual examination of the region suggests the possibility of regional variations. Alternating groups of deposits closer to sandstone-shale contacts and deposits closer to faults occur across the region.

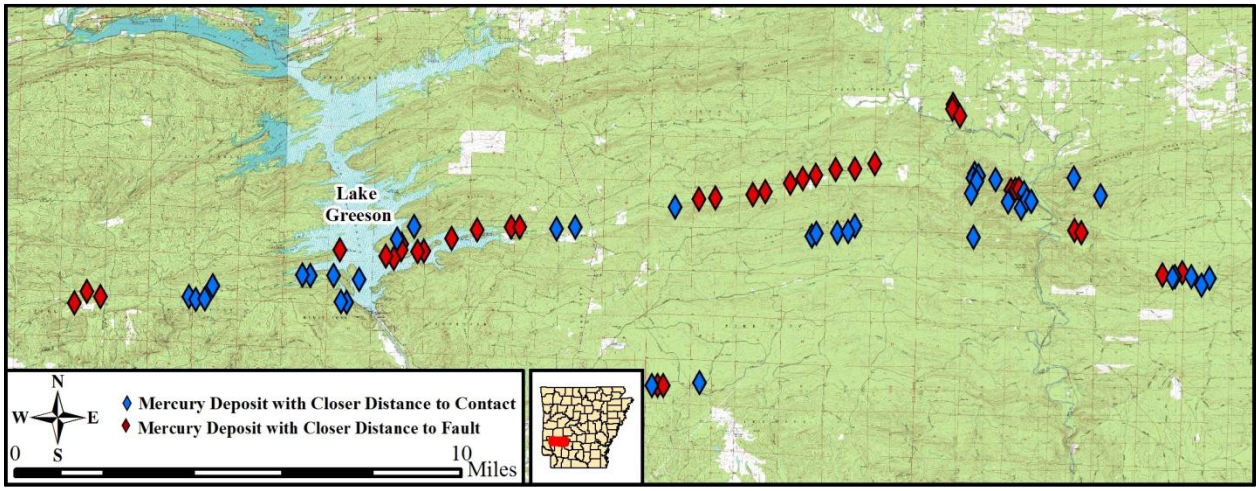

Figure 23.
Map showing the spatial distribution of deposits closer to contacts (blue) and deposits closer to faults (red).

Regional variations were also examined with context to the sandstone and fault composite map (Figure 24). The majority of the deposits that were found to be closer in proximity to a sandstone-shale contact were located within (21) or directly adjacent (20) to an area mapped (via the rock type classification model) as sandstone rather than shale. The majority of the deposits found within areas mapped as sandstone, were associated with the sandstones of the Jackfork Formation. Very few of the deposits found within sandstone regions were associated with sandstones of the Stanley Formation.

The majority of deposits located within the areas mapped as shale were found to be closer to a fault, in particular the major fault traces that span the majority of the study area. The majority of the deposits that were found to be closer to a fault were located within the shale of the Stanley Formation.

Based on the visual examination of the study area, several conclusions can be made about regional variation. Faults appear to be the more controlling mechanism in areas dominated by shale, especially those of the Stanley Formation. The sandstone-shale contacts appear to be the more controlling factor within regions dominated by sandstone, especially sandstone units of the Jackfork Formation.

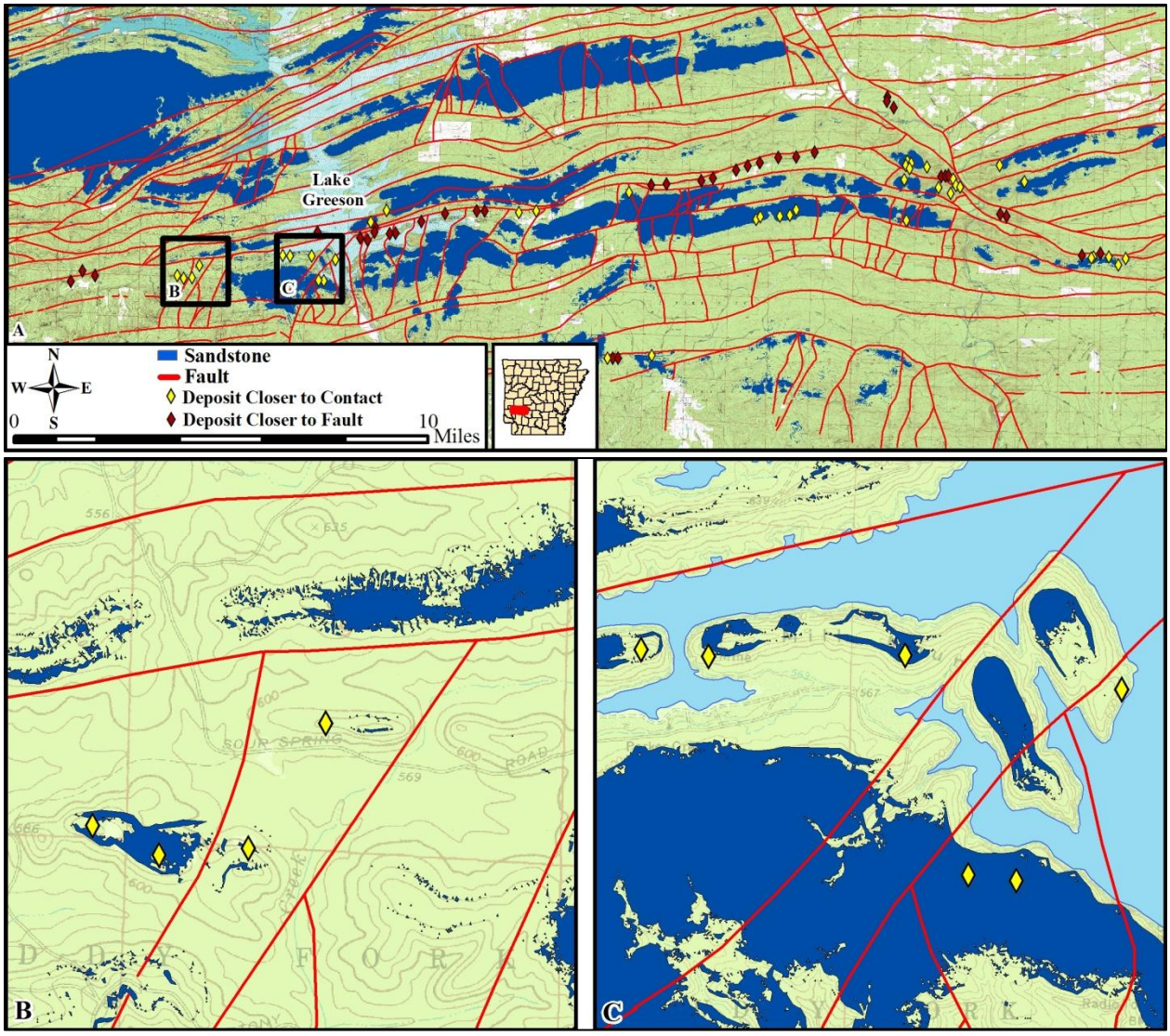

Figure 24.
Map of regional variation across the study area: highlighting faults (red lines), sandstone regions (blue), deposits closer to sandstone-shale contacts (yellow diamonds), and deposits closer to faults (red diamonds). Sandstone regions (blue) not visible at the scale of Map 23A are shown in Maps 23B and 23C.

CHAPTER 12. CONCLUSIONS AND SUGGESTIONS

12.1 Conclusions

The rock type classification model built for this project was successful because it applied the methodology laid out by Belt and Paxton (2005) in a practical, user-friendly, and replicable way. The model also outlined a way for users to remotely map rock type based on the topography. This model combines observations about weathering processes and geomorphology, structure, and the resulting topographic changes when the dominant lithology is either sandstone or shale.

The conclusions of this project relied on the basic assumption that the closer a controlling feature (regional faulting or lithologic change) is to a deposit, the more influence it would have had on the deposit location. Findings showed that the faults have a closer proximity on average to the majority of the deposits, and therefore would have had a greater influence on the deposit location at the time of ore deposition.

Regional variation was also found to be apparent within the region, where in several parts of the district (areas dominated by sandstone) the deposits are closer to sandstone-shale contacts. Conversely, in other parts of the district (areas dominated by shale) the deposit locations are closer to faults. One reason for this occurrence could be that the sandstone is much more fractured and permeable to mineralizing solutions than in the shale regions, allowing for deposition in or near bedding contacts. This is because mineralizing fluids in the region were impermeable to the shale and tended to travel along shale bedding found at lithologic boundaries.

Other reasons for the regional variation could be that in the shale-dominated areas, the majority of fractured zones are in or around fault traces, allowing an avenue for the mineralizing solutions to migrate. This is important because fluid in shale, being unable to penetrate the relatively impermeable rock, depend on fluid avenues (the faulting and fracturing) for transportation and deposition.

Investigation of the regional mercury depositional controls indicated that 41 out of the 77 mercury deposits were closer in proximity to a bedding contact than a fault. The remaining 36 of the 77 mercury deposits were found to be closer to a fault than a bedding contact. Total distances between each deposit and the closest fault and the closest lithologic contact revealed that, on average, faults play a more important role in determining the depositional site.

Both bedding contacts and faults play an almost equally important role in the determination of the depositional site. This project supports what previous work in the region has concluded (Clardy and Bush, 1976; Stearn, 1936; Hansell and Reed, 1935). The combination of the two controlling features is important in understanding the regional depositional site of mercury within this region.

12.2 Suggestions for Prospecting

Future prospecting suggestions for this region would include following within 300 to 350 meters of a sandstone-shale bedding contact within the Jackfork and Stanley Formations in a N80°E direction, following the strike or the alignment of the previously mapped deposits within the region. Also, looking within 200 to 250 meters of a major fault trace, especially bedding plane faults and fault traces found between the Jackfork and Stanley Formations in a N80°E direction may prove beneficial.

12.3 Suggestions for Future Work

The rock type classification model made through this project could have achieved better results if further research in the area of terrain data had been performed. Many more topographic indices exist (such as stream power index and upslope height) than those explored through this project. Suggested work should include investigating alternate topographic attributes or indices that may better indicate changes in rock type, and investigation of the possibility of under-classification of sandstone regions.

The designation of investigation regions used to map the sandstone lithologies in the district need to be further explored. The investigation regions used for this project were extracted from lithologies primarily in the northern portion of the district. The northern portion of the district is composed of sandstones that are found at higher elevations than those sandstones in the southern portion of the district. The slope values of the sandstones in the northern portion of the district are higher than the slope values of the sandstones in the southern portion of the district. Identifying regions adjacent to the deposits may improve classification results. Identifying regions that are more representative of the sandstones of the Stanley Formation may also improve the results of the rock type classification model.

LIST OF REFERENCES

References Cited

Arkansas Geological Commission, 2010, Physiographic regions of Arkansas: available at http://www.geology.ar.gov/education/physio_regions.htm

Arkansas State Land Information Board, 2007, 2006 Fiver Meter Resolution Hillshade Model (raster): available at http://www.geostor.arkansas.gov/G6/Home.html?id=2772e5b64cce0032c96b8a495fd27809, http://www.geostor.arkansas.gov

Aronoff, Stan, 2005, Remote Sensing for GIS Managers, ESRI Press, Redlands, California, 487 p.

Belt, Kevin, and Paxton, Stanley T., 2005, GIS as an aid to visualizing and mapping geology and rock properties in regions of subtle topography: Geological Survey of America Bulletin, v. 117, no.1/2, pp.149-160.

Branner, George Casper, 1932, Cinnabar in southwest Arkansas: Arkansas Geological Commission-Information Circular 2, 51 p.

Clardy, Benjamin F., and Bush, William V., 1976, Mercury district of southwest Arkansas: Arkansas Geological Commission-Information Circular 23, 56 p.

Davis, John C., 2002, Statistics and data analysis in geology: third edition: John Wiley Sons, Inc., New York, New York, 638 p.

Devore, Jay and Farnum, Nicholas, 1999, Applied Statistics for Engineers and Scientists: Duxbury Press, Pacific Grove, California, 577 p.

ESRI 2011. ArcGIS Desktop: Release 9. Redlands, CA: Environmental Systems Research Institute.

Gallagher, David, 1942, Quicksilver deposits near the Little Missouri River, Pike County, Arkansas: U.S. Geological Survey- Bulletin, pp. 189-219.

Hall, Mark, Frank, Eibe, Holmes, Geoffrey, Pfahringer, Bernhard, Reutemann, Peter, and Witten, Ian H., 2009, The WEKA Data Mining Software: An Update; SIGKDD Explorations, Volume 11, Issue 1.

Hansell, J.M., and Reed, J.C., 1935, Quicksilver deposits near Little Missouri River, Southwest Arkansas: American Institute of Mining, Metallurgical and Petroleum Engineers, v. 115, pp. 229-246.

Hatcher, R.D., Jr., Thomas, W.A., Geiser, P.A., Snoke, A.W., Mosher, S., and Wiltschko, D.V., 1989, Alleghanian orogen, in Hatcher, R.D., Jr., Thomas, W.A., and Viele, G.W., eds., The Appalachian-Ouachita Orogen in the United States: Boulder, Colorado, Geological Society of America, The Geology of North America, v. F-2, pp. 233-318.

Makhoul, John, Kubala, Francis, Schwartz, Richard, and Weischedel, Ralph, 1999, Performance measures for information extraction: Proceedings of the DARPA Broadcast News Workshop, Herdon, VA, pp. 249-252.

Miser, H.D., and Purdue, A.H., 1929, Geology of the DeQueen and Caddo Gap quadrangles, Arkansas: U.S. Geological Survey Bulletin 808, 195 p.

Mitchell, Tom. M., 1997, Machine Learning: McGraw-Hill Companies, Inc., 414 p.

Moore, I.D., Grayson, R.B., and Ladson, A.R., 1991, Digital terrain modeling: a review of hydrological, geomorphological, and biological applications; Hydrological Processes, v. 5, pp.3-30.

Morris, R.C., 1989, Stratigraphy and sedimentary history of post-Arkansas Novaculite Carboniferous rocks of the Ouachita Mountains, in Hatcher, R.D., Jr., Thomas, W.A., and Viele, G.W., eds., The Appalachian-Ouachita orogen in the United States: Boulder, Colorado, Geological Society of America, The Geology of North America, v. F-2.

Quinlan, J.R., 1993, C4.5: Programs for machine learning: Morgan Kauffman Publishers, Inc., San Mateo, California, 302 p.

Reed, John C., and Wells, Francis G., 1938, Geology and ore deposits of the southwestern Arkansas quicksilver district: U. S. Geological Survey Bulletin, pp. 15-90.

Sokolova, Marina, Japkowicz, Nathalie, and Szpakowicz, Stan, 2006, Beyond accuracy, f-score and ROC: A family of discriminant measure for performance evaluation: Advances in Artificial Intelligence, v. 4304, pp. 1015-1021

Stearn, Noel H., 1935, Discussion: American Institute of Mining and Metallurgical Engineers, v. 115, pp. 244.-246.

Stearn, Noel H., 1936, The cinnabar deposits in Southwestern Arkansas: Economic Geology, v. 31, no. 1, pp. 1-28.

Stone, Charles G., and Bush, William V., 1984, General geology and mineral resources of the Caddo River Watershed: Arkansas Geological Commission- Information Circular 29, 32 p.

Thomas, William A., 1989, The Appalachian-Ouachita orogen beneath the Gulf Coastal Plain between the outcrops in the Appalachian and Ouachita Mountains, in Hatcher, R.D., Jr., Thomas, W.A., and Biel, G.W., eds., The Appalachian-Ouachita Orogen in the United States: Boulder, Colorado, Geological Society of America, The Geology of North America, v. F-2, pp. 537-553.

Viele, G.W., 1979, Geologic map and cross section, eastern Ouachita Mountains, Arkansas: Geological Society of America Map and Chart Series MC-28F, 8p., scale 1:250,000.

Viele, George W., 1989, The Ouachita Orogenic belt, in Hatcher, R.D., Jr., Thomas, W.A., and Viele, G.W., eds., The Appalachian-Ouachita Orogen in the United States: Boulder, Colorado, Geological Society of America, The Geology of North America, v. F-2, pp. 555-561.

Wilson, John P., and Gallant, John C., 2000, Terrain Analysis: John Wiley and Sons, Inc., New York, 479 p.

APPENDIX

APPENDIX 1

APPENDIX 1. Decision Tree Classification Scheme Output by WEKA

```
DEM <= 212.693
|  SLOPE <= 6.7629
|  |  DEM <= 209.903: shale (41116.0/65.0)
|  |  DEM > 209.903
|  |  |  SLOPE <= 5.2481
|  |  |  |  WET <= 7.6615: shale (591.0/20.0)
|  |  |  |  WET > 7.6615
|  |  |  |  |  WET <= 11.3456
|  |  |  |  |  |  SLOPE <= 3.4593: shale (140.0/7.0)
|  |  |  |  |  |  SLOPE > 3.4593
|  |  |  |  |  |  |  DEM <= 211.893: shale (47.0/13.0)
|  |  |  |  |  |  |  DEM > 211.893
|  |  |  |  |  |  |  |  WET <= 8.329
|  |  |  |  |  |  |  |  |  SLOPE <= 4.2975: shale (3.0)
|  |  |  |  |  |  |  |  |  SLOPE > 4.2975: sandstone (2.0)
|  |  |  |  |  |  |  |  WET > 8.329: sandstone (14.0/1.0)
|  |  |  |  |  WET > 11.3456
|  |  |  |  |  |  SLOPE <= 3.6682
|  |  |  |  |  |  |  WET <= 11.712: sandstone (7.0)
|  |  |  |  |  |  |  WET > 11.712
|  |  |  |  |  |  |  |  WET <= 12.1331: shale (5.0)
|  |  |  |  |  |  |  |  WET > 12.1331
|  |  |  |  |  |  |  |  |  DEM <= 211.465: sandstone (6.0/1.0)
|  |  |  |  |  |  |  |  |  DEM > 211.465: shale (3.0)
|  |  |  |  |  |  SLOPE > 3.6682: sandstone (10.0)
|  |  |  SLOPE > 5.2481
|  |  |  |  WET <= 7.0908
|  |  |  |  |  DEM <= 211.993: shale (85.0/17.0)
|  |  |  |  |  DEM > 211.993
|  |  |  |  |  |  SLOPE <= 6.096: sandstone (13.0/3.0)
|  |  |  |  |  |  SLOPE > 6.096: shale (8.0/2.0)
|  |  |  |  WET > 7.0908
|  |  |  |  |  DEM <= 211.493
|  |  |  |  |  |  PLAN <= 0.9634
|  |  |  |  |  |  |  PLAN <= -0.7814: shale (2.0)
|  |  |  |  |  |  |  PLAN > -0.7814: sandstone (20.0/2.0)
|  |  |  |  |  |  PLAN > 0.9634
|  |  |  |  |  |  |  PLAN <= 1.6522: shale (4.0)
|  |  |  |  |  |  |  PLAN > 1.6522: sandstone (3.0/1.0)
|  |  |  |  DEM > 211.493: sandstone (26.0)
|  SLOPE > 6.7629
|  |  SLOPE <= 11.9479
|  |  |  DEM <= 204.205
|  |  |  |  DEM <= 198.509: shale (1444.0)
|  |  |  |  DEM > 198.509
```

```
|  |  |  |  |  WET <= 6.8658: shale (632.0/32.0)
|  |  |  |  |  WET > 6.8658
|  |  |  |  |  |  SLOPE <= 10.027
|  |  |  |  |  |  |  PLAN <= -0.0062
|  |  |  |  |  |  |  |  WET <= 8.0302
|  |  |  |  |  |  |  |  |  DEM <= 203.607
|  |  |  |  |  |  |  |  |  |  SLOPE <= 7.9684: shale (16.0/1.0)
|  |  |  |  |  |  |  |  |  |  SLOPE > 7.9684: sandstone (8.0/3.0)
|  |  |  |  |  |  |  |  |  DEM > 203.607: sandstone (3.0)
|  |  |  |  |  |  |  |  WET > 8.0302
|  |  |  |  |  |  |  |  |  SLOPE <= 9.3207: sandstone (12.0)
|  |  |  |  |  |  |  |  |  SLOPE > 9.3207
|  |  |  |  |  |  |  |  |  |  DEM <= 201.154: sandstone (2.0)
|  |  |  |  |  |  |  |  |  |  DEM > 201.154: shale (2.0)
|  |  |  |  |  |  |  PLAN > -0.0062
|  |  |  |  |  |  |  |  SLOPE <= 7.6998
|  |  |  |  |  |  |  |  |  DEM <= 198.853
|  |  |  |  |  |  |  |  |  |  PLAN <= 0.6945: sandstone (3.0)
|  |  |  |  |  |  |  |  |  |  PLAN > 0.6945: shale (3.0)
|  |  |  |  |  |  |  |  |  DEM > 198.853: shale (68.0/1.0)
|  |  |  |  |  |  |  |  SLOPE > 7.6998
|  |  |  |  |  |  |  |  |  WET <= 8.5432: shale (75.0/13.0)
|  |  |  |  |  |  |  |  |  WET > 8.5432: sandstone (9.0/3.0)
|  |  |  |  |  |  SLOPE > 10.027: sandstone (27.0/4.0)
|  |  |  DEM > 204.205
|  |  |  |  WET <= 8.095
|  |  |  |  |  DEM <= 208.204
|  |  |  |  |  |  SLOPE <= 9.7149
|  |  |  |  |  |  |  WET <= 5.9378: shale (229.0/22.0)
|  |  |  |  |  |  |  WET > 5.9378
|  |  |  |  |  |  |  |  PLAN <= 0.2367
|  |  |  |  |  |  |  |  |  WET <= 6.8703
|  |  |  |  |  |  |  |  |  |  DEM <= 204.905: shale (12.0)
|  |  |  |  |  |  |  |  |  |  DEM > 204.905
|  |  |  |  |  |  |  |  |  |  |  DEM <= 205.057: sandstone (3.0)
|  |  |  |  |  |  |  |  |  |  |  DEM > 205.057: shale (35.0/9.0)
|  |  |  |  |  |  |  |  |  WET > 6.8703: sandstone (29.0/10.0)
|  |  |  |  |  |  |  |  PLAN > 0.2367: shale (102.0/11.0)
|  |  |  |  |  |  SLOPE > 9.7149
|  |  |  |  |  |  |  DEM <= 206.604: shale (48.0/14.0)
|  |  |  |  |  |  |  DEM > 206.604: sandstone (32.0/6.0)
|  |  |  |  |  DEM > 208.204
|  |  |  |  |  |  DEM <= 210.694
|  |  |  |  |  |  |  SLOPE <= 9.5173
|  |  |  |  |  |  |  |  WET <= 6.5517: shale (71.0/17.0)
|  |  |  |  |  |  |  |  WET > 6.5517: sandstone (37.0/14.0)
```

```
|  |  |  |  |  |  |  SLOPE > 9.5173
|  |  |  |  |  |  |  |  PLAN <= -0.9915: shale (5.0/1.0)
|  |  |  |  |  |  |  |  PLAN > -0.9915: sandstone (44.0/3.0)
|  |  |  |  |  |  DEM > 210.694
|  |  |  |  |  |  |  WET <= 6.1846
|  |  |  |  |  |  |  |  SLOPE <= 7.5533: shale (13.0/5.0)
|  |  |  |  |  |  |  |  SLOPE > 7.5533: sandstone (33.0/3.0)
|  |  |  |  |  |  |  WET > 6.1846: sandstone (65.0)
|  |  |  |  WET > 8.095
|  |  |  |  |  PLAN <= 1.5763: sandstone (176.0/8.0)
|  |  |  |  |  PLAN > 1.5763
|  |  |  |  |  |  DEM <= 210.194
|  |  |  |  |  |  |  SLOPE <= 8.0911: shale (7.0)
|  |  |  |  |  |  |  SLOPE > 8.0911
|  |  |  |  |  |  |  |  PLAN <= 2.3675: sandstone (3.0)
|  |  |  |  |  |  |  |  PLAN > 2.3675: shale (2.0)
|  |  |  |  |  |  DEM > 210.194: sandstone (6.0)
|  |  SLOPE > 11.9479
|  |  |  DEM <= 200.354: shale (77.0/1.0)
|  |  |  DEM > 200.354
|  |  |  |  WET <= 4.771
|  |  |  |  |  SLOPE <= 14.9634
|  |  |  |  |  |  DEM <= 202.906: shale (8.0/2.0)
|  |  |  |  |  |  DEM > 202.906
|  |  |  |  |  |  |  WET <= -1: sandstone (7.0)
|  |  |  |  |  |  |  WET > -1
|  |  |  |  |  |  |  |  WET <= 4.4613: shale (2.0)
|  |  |  |  |  |  |  |  WET > 4.4613
|  |  |  |  |  |  |  |  |  SLOPE <= 12.1815: shale (3.0/1.0)
|  |  |  |  |  |  |  |  |  SLOPE > 12.1815: sandstone (6.0)
|  |  |  |  |  SLOPE > 14.9634: sandstone (24.0)
|  |  |  |  WET > 4.771: sandstone (336.0/3.0)
DEM > 212.693
|  DEM <= 213.293
|  |  SLOPE <= 4.6182
|  |  |  WET <= 8.402
|  |  |  |  SLOPE <= 3.9298: shale (17.0)
|  |  |  |  SLOPE > 3.9298
|  |  |  |  |  SLOPE <= 4.2716: sandstone (2.0)
|  |  |  |  |  SLOPE > 4.2716: shale (3.0)
|  |  |  WET > 8.402: sandstone (14.0/1.0)
|  |  SLOPE > 4.6182: sandstone (160.0/3.0)
|  DEM > 213.293: sandstone (62546.0)
```

APPENDIX 2

APPENDIX 2. Geologic Map References

GEOLOGIC MAP QUADRANGLE	DATE	AUTHOR
Geologic Map of the Athens Quadrangle, Howard, Pike, Montgomery, and Polk Counties, Arkansas	1994	Boyd R. Haley and Charles G. Stone
Geologic Map of the Langley Quadrangle, Montgomery, and Pike Counties, Arkansas	1994	Boyd R. Haley and Charles G. Stone
Geologic Map of the Lodi Quadrangle, Montgomery and Pike Counties, Arkansas	1994	Boyd R. Haley and Charles G. Stone
Geologic Map of the Newhope Quadrangle, Howard and Pike Counties, Arkansas	1994	Boyd R. Haley, Charles G. Stone, William D. Hanson, and Benjamin F. Clardy
Geologic Map of the Center Point NE Quadrangle, Pike and Howard Counties, Arkansas		William D. Hanson, Benjamin F. Clardy, Boyd R. Haley, and Charles G. Stone
Geologic Map of the Narrows Dam Quadrangle, Pike County, Arkansas	1994	Boyd R. Haley, Charles G. Stone, William D. Hanson, and Benjamin F. Clardy
Geologic Map of the Murfreesboro NE Quadrangle, Clark and Pike Counties, Arkansas	1994	Boyd R. Haley, Charles G. Stone, William D. Hanson, and Benjamin F. Clardy
Geologic Map of Chalybeate Mountain West Quadrangle, Pike and Clark Counties, Arkansas	2007	Boyd R. Haley, Charles G. Stone, William D. Hanson and Benjamin F. Clardy
Geologic Map of the Chalybeate Mountain East Quadrangle, Clark County, Arkansas	2007	Boyd R. Haley, Charles G. Stone, William D. Hanson and Benjamin F. Clardy
Geologic Map of the Murfreesboro Quadrangle, Pike and Hempstead Counties, Arkansas	1998	William D. Hanson and Benjamin F. Clardy

Digital Geologic Map of the Delight Quadrangle, Pike County, Arkansas	2000	William D. Hanson, Benjamin F. Clardy, and Jennifer R. Perkins
Geologic Map of the Antoine Quadrangle, Clark and Pike Counties, Arkansas	2000	William D. Hanson, Benjamin F. Clardy, Boyd R. Haley, and Charles G. Stone
Geologic Map of the Okolona North Quadrangle, Clark County, Arkansas	2001	William D. Hanson, Benjamin F. Clardy, and Daniel K. Smith

APPENDIX 3

APPENDIX 3. Distance Database

List of mercury deposits and the straight line distance measured between each deposit and the nearest sandstone-shale contact and the nearest fault. A total of 41 deposits were measured to be closest in proximity to a contact, while the remaining 36 measured closer in proximity to a fault.

Deposit Number	UTM Coordinate (Meters East)	UTM Coordinate (Meters North)	Elevation (Meters)	Distance to Fault (Meters)	Distance to Contact (Meters)
1	438967	3781972	171	178	2147
2	439281	3781975	160	145	1660
3	437745	3781870	176	158	1177
4	436833	3781566	211	430	12
5	435826	3781123	211	164	6
6	435603	3781089	205	126	8
7	434858	3781533	197	273	90
8	435015	3781362	203	288	39
9	434991	3781147	197	379	12
10	434740	3780847	213	213	27
11	434439	3780938	173	246	352
12	432791	3781152	227	164	104
13	432559	3780229	231	338	98
14	431716	3780224	170	86	75
15	431427	3780253	169	134	195
16	433034	3779263	166	83	423
17	432829	3779288	221	177	89
18	433485	3780082	174	55	318
19	435470	3781989	176	29	115
20	440611	3781913	198	104	2
21	441295	3781982	167	22	446
22	444900	3782700	164	163	521
23	445746	3782985	169	166	483
24	446356	3783020	176	101	385
25	447696	3783132	180	151	343
26	448157	3783235	180	149	232
27	449045	3783549	205	108	3
28	449511	3783720	218	63	47
29	449972	3783838	194	136	42
30	449827	3781635	183	134	246
31	449993	3781757	192	151	371
32	450762	3781759	213	131	1

33	451389	3782007	200	50	0
34	451138	3781815	175	10	382
35	450684	3784038	170	15	375
36	451380	3784073	182	106	229
37	452101	3784254	183	168	271
38	455722	3783905	185	174	547
39	455642	3783725	183	173	545
40	455851	3783808	161	200	570
41	455799	3783621	171	149	686
42	455586	3783179	159	156	757
43	457034	3783308	173	106	851
44	457181	3783333	212	668	20
45	457303	3783348	218	577	59
46	456913	3782878	256	699	184
47	457501	3783197	238	706	193
48	457383	3782650	250	546	279
49	457608	3782958	134	373	1753
50	457758	3782896	138	226	1832
51	459312	3781846	132	450	1701
52	459563	3781776	220	104	81
53	455664	3781595	229	342	86
54	460257	3783091	233	165	101
55	463548	3780200	223	360	54
56	464193	3780135	187	146	63
57	462950	3780194	205	337	13
58	463220	3780329	177	414	124
59	462503	3780260	183	293	89
60	462861	3780156	145	104	442
60	463914	3779880	140	175	338
62	454937	3786373	137	247	268
63	454908	3786223	159	201	68
64	444266	3776286	165	276	201
65	445766	3776378	211	81	25
66	423644	3779652	181	101	64
67	424146	3779471	129	240	647
68	423189	3779250	136	267	718
69	427341	3779476	236	241	99
70	427587	3779368	233	387	134
71	427918	3779391	163	62	135
72	428203	3779853	212	181	5
73	444060	3776268	211	140	9

74	444469	3776284	174	13	98
75	455172	3785962	200	83	3
76	456471	3783677	208	371	1
77	459298	3783741	197	81	14

VITA

Lindsey C. Langsdon

BIRTHPLACE:

Birmingham, AL

PERMANENT RESIDENCE:

Germantown, TN

EDUCATION:

M.S. in Engineering Sciences with an emphasis in Geology (August 2011)
The University of Mississippi, *University, MS*

- Research in the use of geospatial and remote sensing applications to geology
- Thesis research used GIS and remote sensing techniques to map geology and investigate spatial distribution of mercury deposits in southwest Arkansas

B.A. in Anthropology, Minor in Geology (Completed in August 2008)
The University of Mississippi, *University, MS*